

Improving Performance Using

Torque Vectoring

on an Electric All-Wheel-Drive Formula SAE Race Car



The REV Project
THE UNIVERSITY OF WESTERN AUSTRALIA



THE UNIVERSITY OF
WESTERN AUSTRALIA

Lochlan Brown

Supervisor: Prof. Thomas Bräunl

Final-Year Thesis submitted for the degree of

Bachelor of Engineering

May 2013

Abstract

Various forms of electronic stability, traction and launch control have existed for over two decades, improving safety, sports performance and off-road capabilities of vehicles. These technologies involve individual control of each wheel's drive torque or braking force in response to the dynamics of the driving conditions and the driver's intentions. With the exception of launch control, applications of these electronic handling-improvement systems are rarely seen on the Formula SAE platform. This is mostly due to the limitations of a combustion engine and conventional drivetrain; individual control of torque to each wheel requires additional mechanical systems adding unjustifiable weight and complexity for the resulting gains. However, an all-wheel-drive electric Formula SAE vehicle with four individual hub motors has the potential for experiments with torque vectoring via electronic means, with minimal additional mechanical systems. The University of Western Australia's Renewable Energy Vehicle (REV) group has been designing such a vehicle for the 2013 Formula SAE competition in Melbourne. Processing driver inputs such as steering angle, throttle and brake position in addition to the actual dynamic state of the vehicle observed through wheel speeds, three axes of acceleration and angular velocities, a torque vectoring algorithm has been designed and implemented on an ARM Cortex M3 microcontroller and has achieved significant improvements in cornering performance.

Contents

1	Introduction	1
1.1	Advantages of Electric Vehicles	1
1.2	The Renewable Energy Vehicle Project	2
1.3	The Formula SAE Competition	3
1.4	2013 Formula SAE car	3
1.5	2010 Formula SAE car	4
1.6	Goals of this Project	4
2	Background Theory and Existing Technology	5
2.1	Forces on a Four-Wheeled Vehicle	5
2.2	Stability	7
2.3	Static Weight Distribution Model	7
2.4	Slip Ratio Control During Acceleration and Braking	8
2.5	Gap in Existing Knowledge	11
3	Algorithm – AWD Torque Vectoring for Formula SAE Car	12
3.1	Stable State Controller	13
3.2	Unstable State Controller	13
4	Hardware	15
4.1	Drive Control Unit (DCU).....	15
4.1.1	Microcontroller Selection	16
4.2	CAN Bus.....	18
4.3	Motors.....	19
4.3.1	Review of PMAC Motor Theory	19
4.3.2	Motors for 2013 Formula SAE Car	20
4.4	Motor Controllers	20
4.4.1	CAN Message Objects	22
4.4.2	Parameter Configuration	23
4.5	Sensors	24
4.5.1	Motor Position Encoder	24
4.5.2	Steering encoder	27
4.5.3	IMU.....	30
4.5.4	Accelerator and Brake Pedals	30
5	Test results	31
5.1	The test procedure.....	31
5.2	Results.....	32

5.3	Conclusions	33
6	Future implementation, Further research and Conclusions.....	34
7	References	35
8	Appendices.....	37
8.1	Extract from BPI-3C1-13 photo interrupter datasheet	37

List of Figures

Figure 1-1: Comparison of Electric Motor Efficiency (left) and Internal Combustion Engine Operating Regions.....	1
Figure 1-2: 2013 AWD Formula SAE Car [15]	3
Figure 1-3: 2010 RWD Formula SAE Car [15]	4
Figure 2-1: Diagram of Forces on a Four-Wheel Vehicle During Cornering [6]	6
Figure 2-2: Cases of Oversteer (left) and Understeer (right)	7
Figure 2-3: Plots of Friction Coefficients vs. Slip Ratio for a Tyre on Various Surfaces [13], [14].....	9
Figure 2-4: Ackermann Geometry and Calculation of Wheel Speeds [13]	10
Figure 3-1: AWD Torque Vectoring Algorithm Flowchart.....	13
Figure 4-1: Arduino Mega based on ATmega1280	16
Figure 4-2: BeagleBoard-xM	17
Figure 4-3: Raspberry Pi.....	17
Figure 4-4: TI Stellaris Cortex-M3 LM3S8962	17
Figure 4-5: PMAC / PMSM / Brushless DC design [16]	19
Figure 4-6: Exploded View of Wheel-Hub Assembly [10]	20
Figure 4-7: Kelly KBL72301X Motor Controller Connections Panel [17].....	21
Figure 4-8: Hall-effect Sensor Placement to Determine Motor Position.....	24
Figure 4-9: Plots of Phase Voltages for Trapezoidal and Sinusoidal PMAC Motor Control Methods [10]	24
Figure 4-10: Hall-effect Motor Position Encoder.....	25
Figure 4-11: Schematic of Hall-effect Sensor Interface	26
Figure 4-12: Oscilloscope Measurements of Hall-effect Encoder Channels.....	26
Figure 4-13: Linear Potentiometer [18]	27
Figure 4-14: Rotary Potentiometer [19]	27
Figure 4-15: Optical Quadrature Steering Angle Encoder	28
Figure 4-16: Encoder Wheel	28
Figure 4-17: Photo Interrupter [20]	28
Figure 4-19: Quadrature Encoder Photo Interrupter Signals.....	29
Figure 4-18: Quadrature Moore Machine	29
Figure 4-20: Schematic of Photo Interrupter with Connections to DCU	30
Figure 4-21: Hall-effect Accelerator Pedal [21]	30
Figure 5-1: Test Track for Cornering Performance	31
Figure 5-2: Plot of Test Results with Torque Vectoring DISABLED	32
Figure 5-3: Plot of Test Results with Torque Vectoring ACTIVATED	33

List of Tables

Table 4-1: Competition scoring - article A1.4.1 [4]	3
Table 9-1: Turnigy CA120-70 PMAC Specifications	20
Table 9-2: Kelly KBL72301X Motor Controller Low Voltage Signals Pin-out and Connections within Vehicle.....	22
Table 9-3: Summary of Most Useful Data Available on the CAN Bus	22
Table 9-4: Quadrature State Table.....	29

Nomenclature

SAE	Society of Automotive Engineers
FSAE-A	Formula SAE – Australasia [competition]
AWD	All-Wheel-Drive
FWD	Front-Wheel-Drive
RWD	Rear-Wheel-Drive
REV	Renewable Energy Vehicle [team]
DCU	Drive Control Unit
CAN	Controller Area Network
ADC	Analogue-to-Digital Converter
PWM	Pulse-Width Modulation
GPIO	General Purpose Input-Output
PMAC	Permanent Magnet Alternating Current
LiFePO ₄	Lithium Ion Phosphate [battery]
SMD	Surface-Mount Device
ICE	Internal Combustion Engine
EV	Electric Vehicle
CM	Centre of Mass
CW	Centre of Weight

1 INTRODUCTION

Recent decades have called for alternative transport options, searching for something more economically and ecologically sustainable. Electric Vehicles (EVs) powered by renewable energy are leading the developments but technology is still in its early days and costs are still extreme. This form of transport is much more efficient and cleaner than Internal Combustion Engines (ICE) though they cannot yet compete on factors like range and convenience.

In many people's minds, EVs might seem exciting, futuristic and innovative but are more often than not, associated with poor performance and range. This is not surprising since exorbitant budgets rarely exist for EV development and sacrifices must be made to favour either performance or range, not both. So perhaps what is needed a shift in the public's focus to high-end, well-funded performance vehicles to show the capabilities of electric cars and then filter in the consumer market later. Indeed, there are even EVs such as the Tesla Roadster Sport capable of outperforming most ICE vehicles (12.64 second ¼-mile).

With the Renewable Energy Vehicle team sharing this vision and SAE International's decision to add an electric class to its Formula SAE design competition, there is opportunity for demonstration of the performance capabilities of electric vehicles. This project specifically focuses on improving handling by using electronic control systems to minimise wheel slip and improve stability. Not only does the project intend to improve performance but also safety by making the vehicle more predictable.

1.1 ADVANTAGES OF ELECTRIC VEHICLES

There are many impressive capabilities of EVs that are either commonly neglected or unknown. In terms of efficiency, electric motors are far more impressive than Internal Combustion Engines.

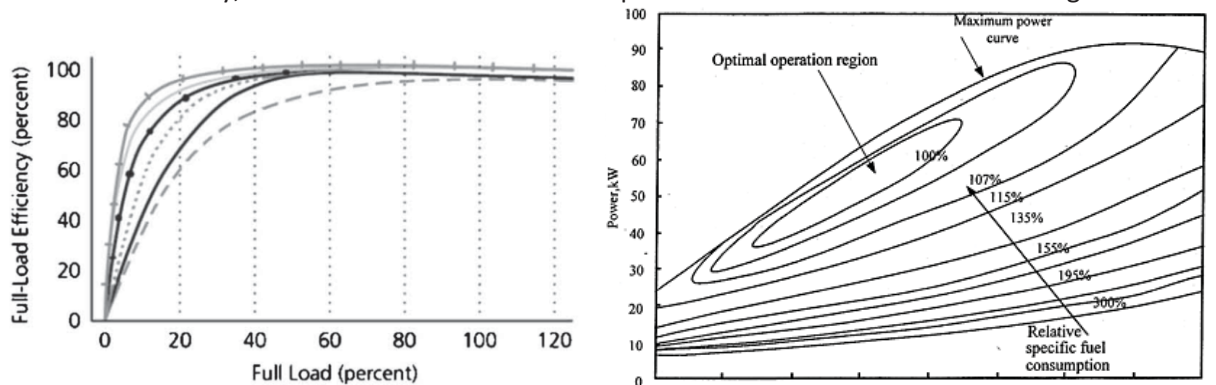


Figure 1-1: Comparison of Electric Motor Efficiency (left) and Internal Combustion Engine Operating Regions

The efficiency of electric motors is typically around 85-95% and this is achieved over most of the motor's load and speed ranges [1]. An internal combustion engine is generally 15-20% efficient, but only at certain loads and speeds. As can be seen in the above, right plot, there is a very narrow optimal operating region [2]. Diesel-electric vehicles recognise this, taking advantage of the range offered by a diesel engine, to turn a generator providing electric power which, in turn, operates an electric motor boasting controllability and efficiency.

More on the lines of effective operating range, most electric motors are capable of producing their rated torque across almost all speeds including, most importantly, from stationary. ICEs are not capable of producing torque from stationary, instead requiring a clutch or similar coupling. The torque and speed of an electric motor are also precisely controllable so that any torque can be demanded for a constant speed and any speed can be demanded for a constant torque (within limits of power rating). This is not the case for ICEs which have also have a much more dependent relationship between torque and speed. The response time to changes of torque demand are also very attractive at around 10ms, compared to ICEs that have delays exceeding 200ms – related to the throttle valve opening, elasticity of air-fuel mixture and inertia of mechanical components [3].

Because of the relatively small size and weight of electric motors, there is greater flexibility for vehicle design. Various numbers of motors and drive setups are possible, such as motors mounted centrally and conventional transmission used, or mounted at the front and rear with axles or even mounted in-wheel without significantly increasing the unsprung mass of the wheel. Different motors can be chosen with very different torque and speed characteristics, depending on the vehicle design and gearing desired. Conventional chassis design is very much limited by size and weight limitations of ICEs and the necessities of their transmission and torque distribution components.

This ability to accurately and quickly control individual wheel torque advocates a wealth of opportunities to experiment with traction control and torque vectoring systems. Furthermore, if any of these systems needed to be changed, it would be a simple matter of a firmware update rather than expensive, time-consuming mechanical redesign. Independent motors for each wheel means complete independent control of every tyre-surface contact patch, not only while driving but also braking.

1.2 THE RENEWABLE ENERGY VEHICLE PROJECT

The Renewable Energy Vehicle (REV) project exists to advocate sustainable, cleaner transport by building zero emission electric vehicles. Certain vehicles target the performance market while others, the commercial or even hobbyist markets. Students and staff from the University of Western Australia fill the variety of responsibilities such as engineering, fabrication, management, marketing and finance.

In 2008, the REV project converted a Hyundai Getz to a fully electric vehicle that can be charged from a standard, single-phase 240 volt power outlet. This vehicle's goal was to meet the daily travel requirements of the average person whilst minimising cost. The conversion of a Lotus Elise, in 2009, prioritised high performance to demonstrate the potential of electric vehicles in multiple markets. Initiation of the West Australian Electric Vehicle Trial, supervised by the REV project, has helped better understand commuting with current electric vehicle capabilities as well as charging habits and the future need for infrastructure. The project is also addressing the issues of charging convenience and range limitations by developing networked charging stations for parking bays. Recently, the REV project has begun designing electric versions of the Formula SAE platform to enter in the Australasia competition.

1.3 THE FORMULA SAE COMPETITION

Since 1978 there has existed a competition organised by SAE International for students to design and manufacture a small Formula race car. Today, universities worldwide compete in a number of these competitions held in various countries. The design and manufacture process must be predominantly student-driven with minimal professional or staff support. Teams and their cars are evaluated in a number of different ways – not only the final car’s performance but also the design process, cost, presentation and issues of safety. Below is the scoring breakdown for the competition.

Static Events:	
Presentation	75
Engineering Design	150
Cost Analysis	100
Dynamic Events:	
Acceleration	75
Skid-Pad	50
Autocross	150
Efficiency	100
Endurance	300
Total Points	1,000

Table 1-1: Competition scoring - article A1.4.1 [4]

Since 2010, the Formula SAE competition has included a fully-electric class. The REV project plans to enter the Formula SAE Australasia competition in Melbourne this year. This project intends to improve the car’s scores in the dynamic events by increasing acceleration with launch control, improving stability on the skid-pad and using regenerative braking to perform well in the efficiency and endurance events. Scoring well in the static events is also important so cost-effectiveness will factor into every design decision.

1.4 2013 FORMULA SAE CAR



Figure 1-2: 2013 AWD Formula SAE Car [15]

The REV project’s 2013 car is an AWD electric car with four in-hub motors. The chassis was designed completely from scratch to best house two pods of batteries and utilise the space not required due to the mounting of motors outside the chassis. The motors chosen were brushless permanent magnet AC outrunners which have a high power to weight ratio and low maintenance. Four Kelly motor controllers, powered by the combined 52 Volt, 8 kWh battery

pods, produce the three phase currents to drive the motors. The vehicle is capable of a peak power output of 60kW (15kW per wheel). It has a theoretical top speed of 110km/h and weighs 280kg.

1.5 2010 FORMULA SAE CAR



Figure 1-3: 2010 RWD Formula SAE Car [15]

The first Formula SAE car the REV project designed was in 2010. It was a conversion using the UWA Motorsport's 2001 chassis. The vehicle's rear wheels are driven by two brushless PMAC motors mounted within the chassis, coupled to the wheels with drive shafts. The maximum power of the 2010 Formula SAE car is 13 kW and is powered by a 48 Volt, 4.3 kWh battery pack.

1.6 GOALS OF THIS PROJECT

The specific aim of this project is to improve performance of an AWD Formula SAE car, all-round, by designing a system that implements stability control, wheel slip regulation, launch control and ABS. The intention is to achieve this with minimal complexity and high cost-effectiveness. In the context of the FSAE-A competition, the goals are to enter a car into the competition and improve the car's score in the acceleration, skid-pad and endurance events while not sacrificing scoring in the cost analysis event.

More generally, this project hopes to advocate for the viability of electric vehicles. By producing a vehicle capable of outperforming a similar class ICE vehicle, the view of some that electric vehicles are slow and unusable can be challenged.

2 BACKGROUND THEORY AND EXISTING TECHNOLOGY

Various traction control systems have existed for decades both mechanically, in the form of differentials and electronically in the form of ABS and ESC, to name a few. There has been a considerable amount of research into traction control algorithms including some projects that have taken advantage of electric vehicles. The following is a summary of some of the existing technology on which this project will be based.

2.1 FORCES ON A FOUR-WHEELED VEHICLE

Ignoring driving resistances related to rolling and aerodynamics, the basic force acting on a four-wheel vehicle is a torque producing a longitudinal horizontal force on the road surface with a reaction from the surface acting on the vehicle through the axle bearings. The other important force is parallel to the wheel's axis of rotation – the lateral force. This force is a reaction to the tyres' side-slip force and allows the vehicle to steer. Both longitudinal and lateral forces are limited by the tyre's friction coefficient, defining maximum shear force on the contact patch between tyre and road surface.

These forces are not necessarily balanced or consistent and cannot be controlled for tyres that are not driven. Exceeding maximum friction force is therefore not often predictable, resulting in dangerous situations such as understeering in a front-wheel-drive car or oversteering in a rear-wheel-drive car [3].

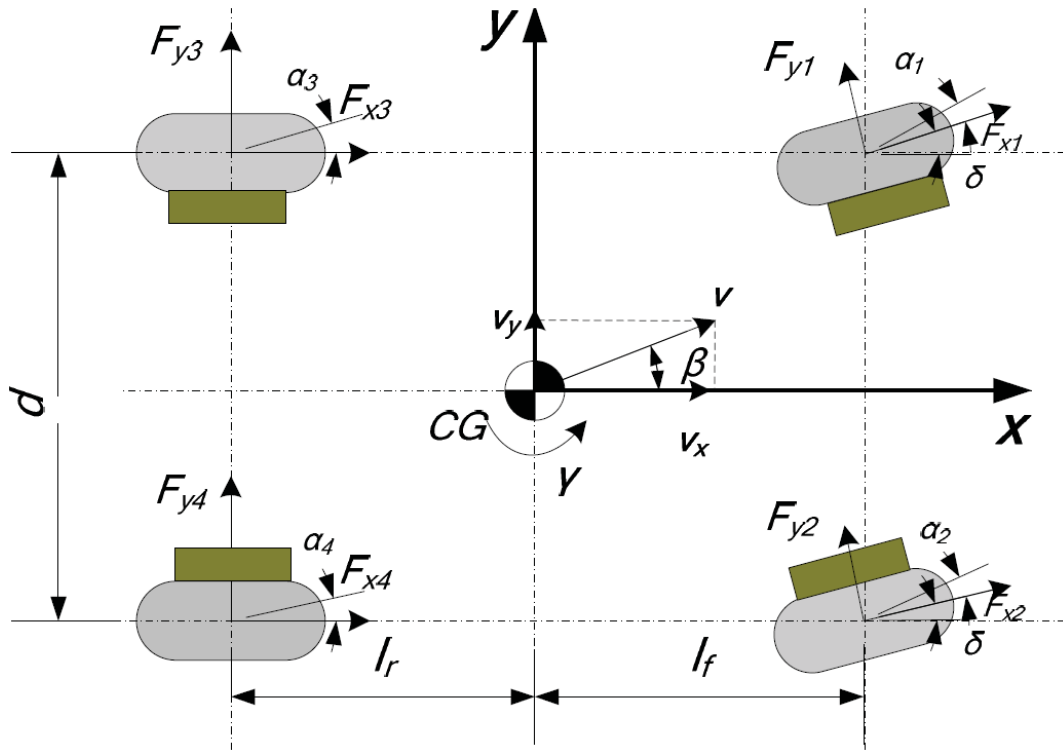


Figure 2-1: Diagram of Forces on a Four-Wheel Vehicle During Cornering [6]

The forces acting on the vehicle according to the above figure can be summarised as follows [5], [6]:

$$mv(\dot{\beta} + \gamma) = F_{y1} + F_{y2} + F_{y3} + F_{y4} \quad (2-1)$$

$$I_z \dot{\gamma} = l_f(F_{y1} + F_{y2}) - l_r(F_{y3} + F_{y4}) + \frac{d}{2}(F_{x2} - F_{x1} + F_{x4} - F_{x3}) \quad (2-2)$$

Where m is the vehicle's mass, v is the vehicle's linear velocity, β the body side-slip angle, γ the yaw rate, F_{xi} and F_{yi} the longitudinal and latitudinal forces on the tyres, I_z the vehicle inertia about the Z-axis, l_f and l_r the distances of the CM from the front and rear axles and d the wheel base. Body side-slip angle can be estimated using:

$$\beta = \arctan\left(\frac{v_y}{v_x}\right) \quad (2-3)$$

Where v_x is the longitudinal velocity calculated from wheel speed measurements and v_y is obtained through integration of lateral acceleration. Tyre side-slip angle can also be calculated, from steering angle δ :

$$\alpha_1 = \alpha_2 = \beta + \frac{l_f \gamma}{v} - \delta \quad (2-4)$$

$$\alpha_3 = \alpha_4 = \beta - \frac{l_r \gamma}{v} \quad (2-5)$$

2.2 STABILITY

Mathematically, the goal of the torque vectoring system in terms of stability is to minimise S in the following equation:

$$S = |\gamma_{des} - \gamma| + |\beta_{des} - \beta| \quad (2-6)$$

Where $\gamma_{des} - \gamma$ and $\beta_{des} - \beta$ represent the difference between desired and actual yaw rate, and the difference between desired and actual body slip, respectively [7]. A significant discrepancy between desired yaw rate γ and actual yaw rate γ_{des} can result in a loss of stability. This is observable in cases of understeer or oversteer. A vehicle that is understeering has a lower actual yaw rate than desired yaw rate. Oversteering is the opposite, with a higher actual yaw rate, generally resulting in spin-out.



Figure 2-2: Cases of Oversteer (left) and Understeer (right)

For yaw error e_γ to be calculated, the driver's desired yaw rate must be determined from steering angle and current vehicle speed [6]:

$$\gamma_{des} = \frac{v\delta}{l_f + l_r} \quad (2-7)$$

$$e_\gamma = \gamma_{des} - \gamma \quad (2-8)$$

$$e_\gamma = \frac{v\delta}{l_f + l_r} - \gamma \quad (2-9)$$

The yaw error can be minimised by creating an assisting yaw moment. As can be seen in equation (3-2), the longitudinal forces on the tyres can change the inertia moment about the CM Z-axis. Changing these longitudinal forces simply involves vectoring different torque to each wheel using a closed loop system. The measured yaw rate is the feedback and the yaw error is the control variable [8].

2.3 STATIC WEIGHT DISTRIBUTION MODEL

The location of the centre-of-mass (CM) of a vehicle is consistent and determined by the chassis construction. The centre-of-weight (CW) location of a vehicle changes depending on the forces it

experiences. Due to the design of a vehicle, its CM and CW are located above the ground. However, the forces on a vehicle originate from the contact between tyres and road surface. This means all forces on the vehicle result in moments generated about the CM. The sum of these moments result in a body-roll and shift of the CW location with respect to the CM. This weight transfer causes a change in down-force on each wheel which affects the total longitudinal and latitudinal forces the wheel is capable of exerting without losing traction.

$$F_{trans_x} = a_x M \frac{h_g}{l}$$

$$F_{trans_y} = a_y M \frac{h_g}{d}$$

(2-10)

Where F_{trans_x} and F_{trans_y} are the weight transfer equations in the longitudinal and lateral axes respectively, a_x and a_y the acceleration, M the vehicle mass, d and l the track width and wheelbase, and h_g the height of the CM. Additionally, roll stiffness of front and rear are ρ_f and ρ_r , and distance of front and rear axle from CM are l_f and l_r . The vertical down-force on each wheel then becomes [9]:

$$F_{zfl} = \frac{1}{2} \frac{l_r}{l} Mg - \rho_f a_y M \frac{h_g}{d_f} - a_x M \frac{h_g}{l}$$

$$F_{zfr} = \frac{1}{2} \frac{l_r}{l} Mg + \rho_f a_y M \frac{h_g}{d_f} - a_x M \frac{h_g}{l}$$

$$F_{zrl} = \frac{1}{2} \frac{l_f}{l} Mg - \rho_r a_y M \frac{h_g}{d_r} + a_x M \frac{h_g}{l}$$

$$F_{zrr} = \frac{1}{2} \frac{l_f}{l} Mg + \rho_r a_y M \frac{h_g}{d_r} + a_x M \frac{h_g}{l}$$

(2-11)

The prediction of how much torque should go to each wheel can be based on the ratios between down-force which are likely to be good predictions of traction forces available.

2.4 SLIP RATIO CONTROL DURING ACCELERATION AND BRAKING

In order to achieve ultimate performance, the force between the tyre contact patch and the road surface must be maximised without introducing excess wheel slip. With ideal surfaces, there is a maximum friction force F_f related to the static coefficient of friction μ_s and normal force F_N that prevents movement parallel to the contact area.

$$F_f = \mu_s F_N$$

(2-12)

The surfaces move across each other once this force is exceeded and the resistive force is no long related to the static coefficient of friction, but instead, the dynamic coefficient of friction, μ_k . This resistive force during movement is usually less than that while stationary (since the dynamic coefficient is usually less than the static coefficient).

In the case of rubber tyres, the forces are much more complex due to tyre deformation. The scope of this project does not cover the mechanics of materials interaction such as the Pacejka “Magic Formula” tyre model, as knowledge of the physics is not necessary. However, awareness of the changing tyre coefficient of friction and the ability to use a lookup table based on experimental data to electronically control wheel slip is within the scope of this project. Contrary to intuition based on the above ideal static and dynamic states with their related coefficients of friction (equation 3-2), a small amount of relative slip between tyre and road surface actually increases coefficient of friction. Tyre slip ratio S_r is defined as the ratio between the actual speed of the wheel ω and the speed the wheel would be rotating if it had traction (calculated from vehicle velocity v and tyre radius r) [3].

$$S_r = \frac{\omega - \frac{v}{r}}{\frac{v}{r}} \quad (2-13)$$

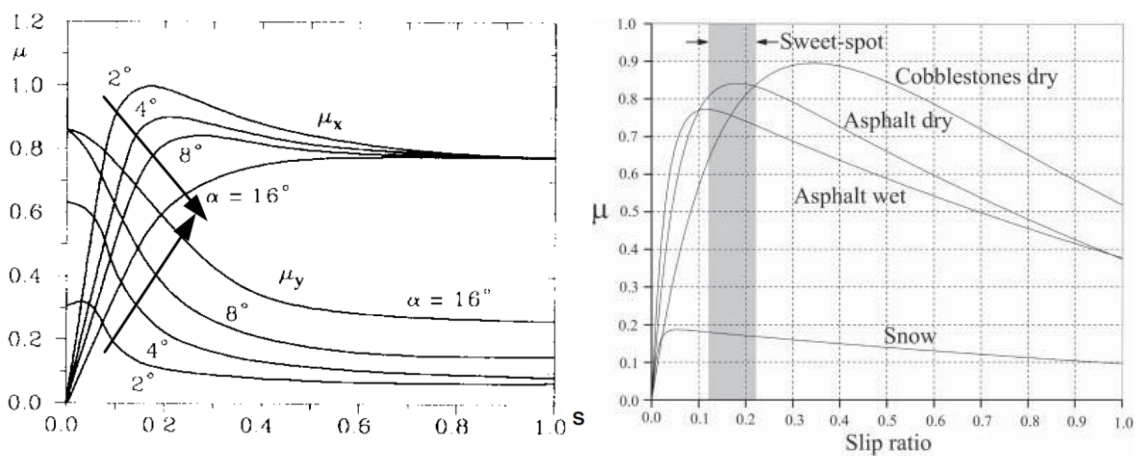


Figure 2-3: Plots of Friction Coefficients vs. Slip Ratio for a Tyre on Various Surfaces [13], [14]

As can be seen in the above figures, showing similar data from two different sources, the optimum friction coefficient for the average tyre actually occurs with a reasonable amount of slip – over the approximate range $S_r \in [0.08, 0.22]$. The slip ratio can be maintained within this range using a software closed loop control system, where torque demand is regulated by the error between desired and actual wheel slip ratio and wheel speed measurement provides the feedback loop.

The main advantage of controlling the slip ratio and improving longitudinal traction is the ability to achieve maximum acceleration from stationary – “launch control”. As is the case for many types of electric motors, maximum torque is available from stand-still so the likelihood of traction loss is high. Conventional methods of launch control in ICE vehicles involve immediately reducing torque to the wheels when a particular limit of tolerated wheel slip is exceeded [3]:

- **Engine Torque Limiting**

Engine torque is suppressed by temporarily cutting off air or fuel supply, or by dropping the spark for a few cycles so the engine fails to fire.

- **Clutch Engagement Control**

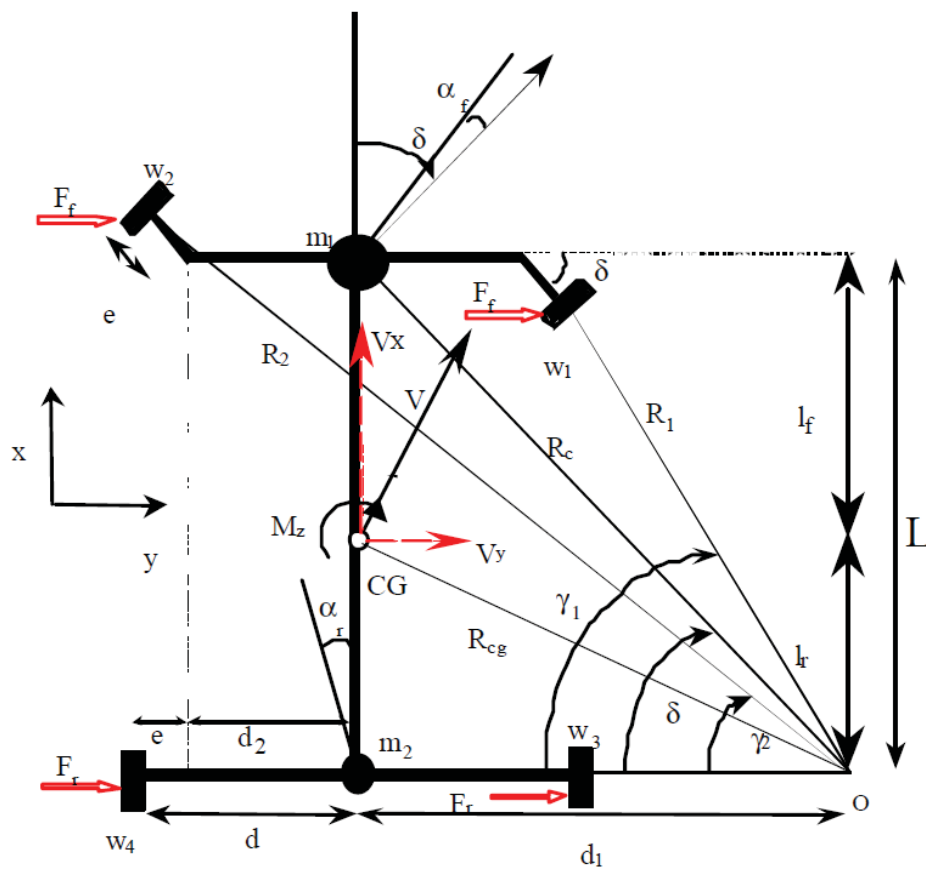
An actuator on the clutch can override driver input to regulate torque by varying clutch plate slippage. Poor accuracy of control and reduced clutch lifetime are disadvantages.

- **Brake Force Application**

Without changing drive torque, brakes can be applied to any wheels exceeding maximum allowed wheel slip ratio. Generally faster response and more accurate than engine torque limiting but overuse of brakes can result in thermal problems.

- **Limited-slip Differential (mechanical-only solution)**

Limited-slip differentials (LSDs) are mechanical components that transfer torque from one source to two axels and allow only a small difference in wheel speed between left and right axel. The LSD mechanically transfers torque to the slower wheel which generally prevents loss of traction where one wheel has a much lower coefficient of friction. However, it doesn't prevent both wheels losing traction and slipping at a similar speed.



$$\begin{cases} \Omega_1 = \frac{L + \text{sign}(\delta) \cdot e \cdot \sin|\delta| \cdot \sin|\delta|}{L \cdot \sin|\gamma|} \cdot \Omega_{c_av} \\ \Omega_2 = \frac{L - \text{sign}(\delta) \cdot e \cdot \sin|\delta| \cdot \sin|\delta|}{L \cdot \sin|\alpha|} \cdot \Omega_{c_av} \\ \Omega_3 = \frac{L \cdot \cos|\delta| + \text{sign}(\delta) \cdot d \cdot \sin|\delta|}{L} \cdot \Omega_{c_av} \\ \Omega_4 = \frac{L \cdot \cos|\delta| - \text{sign}(\delta) \cdot d \cdot \sin|\delta|}{L} \cdot \Omega_{c_av} \end{cases}$$

Figure 2-4: Ackermann Geometry and Calculation of Wheel Speeds [13]

Launch control with torque regulated by electric motors capable of fast, precise response solves many of these disadvantages and mechanical complexities (at the expense of electronic and software complexity). Not only can wheel slip ratio control be useful to maximise acceleration but also to improve braking performance. An ABS-like system can control the amount of regenerative braking force to maintain the individual wheel slip ratios in the region of optimum friction coefficient.

In order to control wheel slip ratio, a prediction of individual desired wheel speeds must be made. This can be based on current wheel speeds and the calculated Ackermann relationship between wheel speeds as constrained by the chassis and steering system. Using these predictions of wheel speeds $\Omega_{1..4}$ and comparing to actual measured wheel speeds, discrepancies in slip ratio can be detected and controlled to remain below 0.22.

2.5 GAP IN EXISTING KNOWLEDGE

There is a lot of literature on traction control, stability control, launch control, torque vectoring, ABS and all related technologies that are based on the concepts of improving tyre-surface interaction for the purpose of safety and performance. Recently, more literature is appearing on electric vehicle traction systems, particularly 2WD, as new technology is enabling exposure in this area. However, there is a lack of research into electric AWD vehicles and any of the publications related to this platform are generally limited to simulations. This may be because the new technologies are expensive to develop, particularly AWD vehicles and few have access to the resources. The REV students are lucky enough to have these opportunities, even though budget is limited.

Naturally, there are many Formula SAE publications on all manner of torque and traction related concepts, but the electric vehicle class is new and teams generally don't choose the AWD option. For this reason, there is certainly a knowledge gap that can be filled about the effectiveness of torque vectoring on the electric Formula SAE platform, as improvements in performance are always welcome in a competitive situation.

Research in the area may even prove that the technologies are expensive, wasteful on space and not capable of observable improvements worth the research time. This is often the conclusion of the ICE class of Formula SAE teams, though it is usually because the traction systems involve mechanical components that add significant size and weight.

3 ALGORITHM – AWD TORQUE VECTORING FOR FORMULA SAE CAR

The algorithm designed for the AWD independent hub-motor vehicle consists of two main control concepts – the “stable” state controller and the “unstable” state controller. The stable controller assumes the vehicle has negligible wheel slip and minimal yaw rate error. It estimates appropriate torque split to the four wheels based on steering demands and calculations of weight transfer. The unstable controller monitors the vehicle state and responds to a loss of stability or excessive wheel slip. Each of these controller components output four scaling parameters – one for each wheel – that default to a value of 1.0. The torque distributor simply multiplies each of the wheel’s two respective scaling factors K_{stable} and $K_{unstable}$ by the driver’s throttle input P_{th} to get a unique percentage of maximum torque for each motor controller, τ .

$$\% \tau_{rr} = \frac{P_{th} K_{stable_{rr}} K_{unstable_{rr}}}{P_{th_{MAX}}}$$

$$\% \tau_{rl} = \frac{P_{th} K_{stable_{rl}} K_{unstable_{rl}}}{P_{th_{MAX}}}$$

$$\% \tau_{fr} = \frac{P_{th} K_{stable_{fr}} K_{unstable_{fr}}}{P_{th_{MAX}}}$$

$$\% \tau_{fl} = \frac{P_{th} K_{stable_{fl}} K_{unstable_{fl}}}{P_{th_{MAX}}}$$

(3-1)

Where $P_{th_{MAX}} = 1023$ for the throttle position connected to a 10-bit ADC input and mapped to full range to compensate for dead-zones.

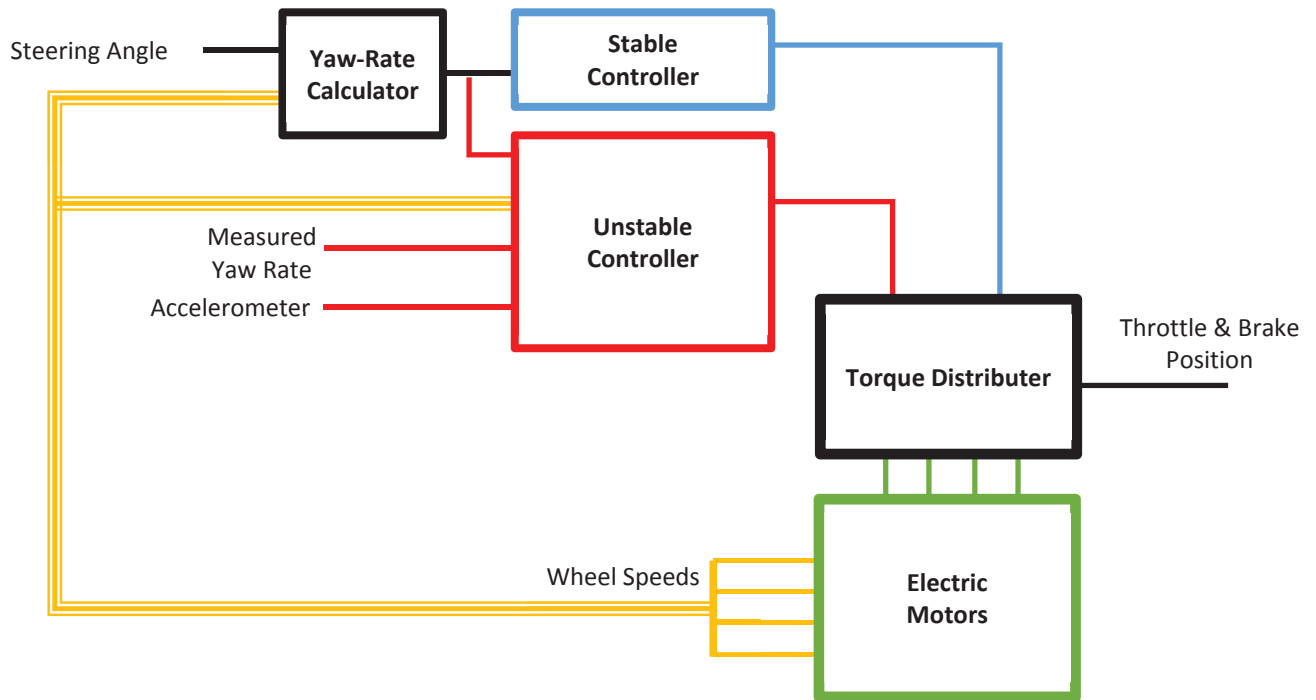


Figure 3-1: AWD Torque Vectoring Algorithm Flowchart

3.1 STABLE STATE CONTROLLER

The main responsibility of the stable state controller is to calculate the normal forces on each of the four wheels. This ensures torque is vectored appropriately to those tyres with enough traction to apply the resultant force to the road. Weight transfer was covered in section 2.3 and those calculations are implemented in the stable controller.

Torque is scaled according to the ratio between estimated immediate dynamic down-force and static down-force (which is precisely 25% of the vehicle's weight since weight distribution is 50:50 on in both axes).

$$K_{stable_{rr}} = 4K_t \frac{F_{zrr}}{M}$$

$$K_{stable_{rl}} = 4K_t \frac{F_{zrl}}{M}$$

$$K_{stable_{fr}} = 4K_t \frac{F_{zfr}}{M}$$

$$K_{stable_{fl}} = 4K_t \frac{F_{zfl}}{M}$$

Where K_t is an experimentally variable factor, M is the vehicle mass of 280kg and the four estimations of down-force $F_{z_}$ are defined in equation (3-11).

3.2 UNSTABLE STATE CONTROLLER

The unstable state controller constantly updates the yaw rate error – see equation (3-8) Based on the desired and actual yaw rates, the following case structure is implemented:

Oversteer Case: $|\gamma| > |\gamma_{des}|$

The actual yaw rate is greater than the desired yaw rate. Therefore the vehicle is oversteering and a yaw moment needs to be generated in the opposite direction. The torque-scaling factors are calculated as follows:

$$\begin{bmatrix} K_{unstable_{rr}} \\ K_{unstable_{rl}} \\ K_{unstable_{fr}} \\ K_{unstable_{fl}} \end{bmatrix} = \begin{bmatrix} 1 + K_{P_{rr}} e_\gamma \\ 1 - K_{P_{rl}} e_\gamma \\ 1 + K_{P_{fr}} e_\gamma \\ 1 - K_{P_{fl}} e_\gamma \end{bmatrix}$$

The error is multiplied by proportional factors $K_{P_}$ that can be determined by experimentation. The output parameters $K_{unstable_}$ are subtracted from or added to 1 as appropriate so that the torque is vectored in favour of the inner wheels not the outer. Whether the desired yaw rate is clockwise, $e_\gamma = \gamma_{des} - \gamma > 0$, or anticlockwise, $e_\gamma = \gamma_{des} - \gamma < 0$, the above equations hold as the sign of e_γ reverses.

Understeer Case: $|\gamma| < |\gamma_{des}|$

The actual yaw rate is less than the desired yaw rate so the vehicle is understeering. An assistive yaw moment needs to be generated.

$$\begin{bmatrix} K_{unstable_{rr}} \\ K_{unstable_{rl}} \\ K_{unstable_{fr}} \\ K_{unstable_{fl}} \end{bmatrix} = \begin{bmatrix} 1 + K_{P_{rr}} e_\gamma \\ 1 - K_{P_{rl}} e_\gamma \\ 1 + K_{P_{fr}} e_\gamma \\ 1 - K_{P_{fl}} e_\gamma \end{bmatrix}$$

Wheel slip is also corrected by the unstable controller. The algorithm integrates accelerometer data to calculate vehicle speed. It then uses Ackermann geometry to predict the different speeds of each of the wheels (which are significantly different during cornering). The measured wheel speeds are then compared to the predicted wheel speeds to see if all are within the wheel slip ratio tolerance of 0.08 to 0.22 (see section 2.4). If they are beyond the upper limit, the previously calculated scaling factors $K_{unstable_}$ are then multiplied by $\frac{1}{K_s(1+S_r)}$ which corrects for the slip and includes a scaling factor K_s to vary the significance of its affect.

Since integrating accelerometer data will gradually accumulate error and become inaccurate, a reset feature has been incorporated into the algorithm. If the measured wheel speeds are zero or near-zero, the vehicle is assumed to have traction so the measured wheel speeds would be an accurate representation of the vehicle's velocity – therefore the integrator value is reset to the measured wheel speeds. Similarly, if the accelerometer data is showing only small forces on the vehicle and the steering angle is near centre then it is assumed the vehicle is not braking heavily, nor accelerating heavily, nor cornering or any other manoeuvre that would suggest wheel slip is significant. This would also suggest the measured wheel speeds are accurate and the integrator can be reset to the calculation of vehicle velocity based on the measured wheel speed values.

4 HARDWARE

4.1 DRIVE CONTROL UNIT (DCU)

The computational centre of the torque vectoring system is the microcontroller-based drive control unit. The microcontroller is responsible for all signals processing, torque vectoring calculations, sending torque demands to motor controllers and data logging. In order to fulfil these tasks, the following requirements were devised to choose a microcontroller.

- **Fast clock speed**

In order to achieve all the above tasks and respond in real-time to the vehicle's rapidly changing traction state, fast processing speed is required.

- **Serial communication (UART)**

PC diagnostics and external logging would require RS232 communication. Additional features such as a driver heads-up display, or GSM modem for trackside monitoring would use UART peripherals.

- **Analogue-to-Digital Converter (ADC)**

Throttle, brake and IMU inputs are analogue 0-5 volt signals requiring accurate ADC conversion. Future implementation of sensors for temperature or battery voltages could also make use of ADC peripherals.

- **Controller Area Network (CAN Bus)**

CAN bus is standard in most vehicles and allows microcontrollers to communicate on a shared bus without a host. The motor controllers have a range of data values reflecting motor and battery state available over CAN bus – most importantly, rotational speed. A CAN-enabled system will also allow for future expansion and additional devices without additional communication complexity.

- **Digital-to-Analogue Converter (DAC) or Pulse-Width Modulation (PWM)**

Some motor controllers can receive throttle input as a CAN signal, which would be the ultimate method of controlling the torque of each motor. However, most only have a 0 to 5 volt signal input for a standard three-wire potentiometer or Hall-effect sensor. A microcontroller with DAC hardware could generate these signals most accurately, though a PWM module would be equally effective provided the frequency is high enough for the controller's internal high-pass filtering on the throttle input.

- **External memory access (SD card or USB memory)**

For data logging, the DCU would preferably have SD card or USB host peripherals to enable removable storage. This would improve ease of access and portability, compared to on-board EEPROM storage, for example. Logging to an external device or PC over serial communication would be an alternative.

- **Floating-point arithmetic**

Not essential. Although with trigonometric calculations and the potential for consecutive carrying of rounding errors, floating point capability is a simple way to improve range and precision while maintaining coding simplicity.

4.1.1 Microcontroller Selection

Many embedded solutions were considered for the DCU based on the above requirements. Not only were the hardware requirements matched but also comparisons were made of cost, extent of support for ease of programming and appropriateness for use in automotive applications. The following is a summary of the most significant solutions considered.

Arduino



Figure 4-1: Arduino Mega based on ATmega1280

Based mostly on the Atmel 8-bit AVR core and some 32-bit ARM versions, the Arduino is popular and versatile tool for common, basic microcontroller projects. Advantages include easy-to-use libraries and extensive support, although the language is somewhat high-level and the Arduino compiler has its limitations for the more specific tasks. Most boards can achieve 16 DMIPS (Dhrystone Million Instructions per Second), have many channels of 10-bit ADC, a PWM module and

communications such as UART, SPI and I²C. However, to enable CAN bus communications, an additional standalone CAN controller and transceiver would have to be interfaced. Additionally, there is very limited on-board EEPROM for data logging, which in itself is an inconvenient storage option as it requires a PC uploading process to retrieve data. External hardware would need to be interfaced for additional storage space.

BeagleBoard

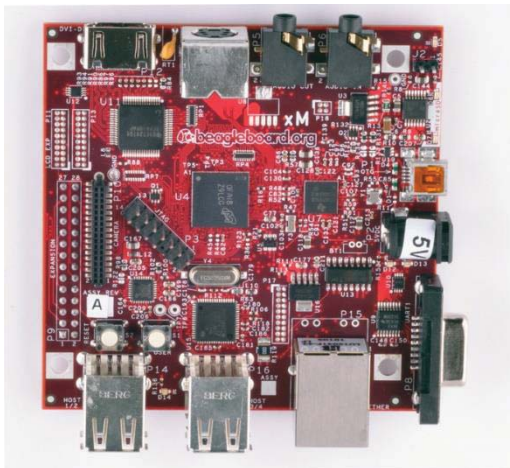


Figure 4-2: BeagleBoard-xM

A low-power, single-board computer has the advantage of convenience – ready to use straight out of the box. The PC graphics interface simplifies the programming and debugging process and also allows for easy development of a complete diagnostics or driver display. With a 1GHz ARM Cortex-A8 core capable of over 1200 DMIPS and floating-point arithmetic, real-time processing capability is of no concern. There are multiple memory options for data logging including on-board NAND flash, a USB host and SD/MMC access. All required communication peripherals, ADC and PWM are all available either on the main board or on the separate “capes” (expansion boards) that can be purchased for the BeagleBoard. However, using

multiple piggy-back expansion boards becomes very expensive and large compared to other embedded alternatives. Ultimately, though this system meets most of the requirements for the DCU, it is more useful for experimentation only. A consequence of torque distribution algorithm running within a full operating system is excessive, unnecessary bloatware and is uncommon for automotive applications.

Raspberry Pi

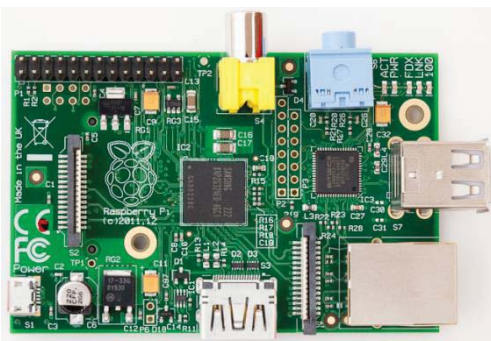


Figure 4-3: Raspberry Pi

Also a single-board computer, the Raspberry Pi is extremely cheap and slightly smaller than the BeagleBoard. It has similar performance, storage options and peripherals but does lack ADC, PWM and CAN Bus – requiring additional hardware interfaced with I²C, SPI or UART. In terms of size and cost, it might be a better alternative to the BeagleBoard but similarly has an undesirable superfluous operating system. It would be most useful if graphics capabilities for diagnostic or driver displays was a priority.

ARM Cortex-M core



Figure 4-4: TI Stellaris Cortex-M3 LM3S8962

The Cortex-M series of 32-bit RISC ARM cores intended for microcontroller applications are common architectures and are manufactured by many companies including Cypress Semiconductor, Energy Micro, Infineon Technologies, Texas Instruments, NXP Semiconductor and STMicroelectronics. The Cortex-M3 and Cortex-M4 are capable of 60 to 150 DMIPS depending on the variant chosen and have a lot of support for development. Evaluation

boards are reasonably cheap and provide easy access to all required communication peripherals including two separate CAN bus controllers. ADC (12-bit on the Cortex-M4) and PWM are standard, in addition to SD card access and a host controller for USB memory storage. An additional feature is a quadrature module that uses dedicated hardware interrupts and software libraries to process AB encoder inputs. The Cortex-M4 is specifically designed for real-time digital signals processing and the ARM cores are frequently used in automotive applications. As a comprehensive, single chip with all the required peripherals and features, the Cortex-M would be the best choice for the DCU. The Cortex-M3 is slightly cheaper and would be sufficient as the additional performance of the Cortex-M4 is nonessential.

MIPS M4K core

The PIC32 microcontrollers from Microchip and the Cortex-M microcontrollers have almost identical performance and features. The MIPS M4K cores are much less widely used than the ARM cores which reduces support and likelihood of finding similar applications. Cost and size are similar.

Infineon

Infineon designs many microcontrollers commonly used in automotive applications such as engine management and vehicle safety systems. The TriCore 32-bit microcontroller also has many of the same features as the MIPS and Cortex-M cores, but with slightly better performance. However, there is much less community support and the significantly higher cost is unjustifiable when the Cortex-M microcontrollers are sufficient.

The Texas Instruments Stellaris Cortex-M3 was determined to be the most suitable, considering the DCU requirements, cost effectiveness and ease of development. Automotive applications are common for this core and minimal additional hardware is required for the DCU's functions. A variety of toolchains are available for programming the microcontroller, such as Keil μ Vision and CodeSourcery. These enable convenient debugging and problem solving, as does the small but practical, on-board LCD screen.

4.2 CAN Bus

In automotive systems there can be many sensors making data available and many devices that need access to sensor data. Rather than designing an excess of individual communications methods, Bosch developed a network for all devices to share, and the technology is now standard on almost all vehicles. CAN bus is a message-based protocol where any node can broadcast a message object on the network containing the data and a unique ID. Another node can choose to listen for that ID and receive any data associated with it. The result is a physically simple, low cost communication protocol that can easily connect many devices.

The hardware requirements of the CAN bus are, in its most basic form, three wires – ground, CAN-high and CAN-low. Any node with a CAN transceiver peripheral can tap into these wires and broadcast or receive data. The bus should be terminated at each end with a 120 Ω resistor to avoid signal reflections. The bus operates at 1Mbit/sec which has a limited bus length of 25 meters and utilises the CANopen protocol.

4.3 MOTORS

4.3.1 Review of PMAC Motor Theory

The following is a very simplistic summary of brushless permanent magnet AC (PMAC) technology that is necessary to explain controller setup and sensor design in the following sections. This type of electric motor is also referred to as a brushless DC (BLDC) motor or a permanent magnet synchronous machine (PMSM). All terms reflect the same mechanical design – a stator with phase windings that produce a rotating magnetic field by energising in sequence, and a rotor with a number of permanent magnets alternating in orientation. Most commonly, the rotor spins within the stator, though in some cases the stator is in the centre with a ring or “can” of magnets rotating around the windings.

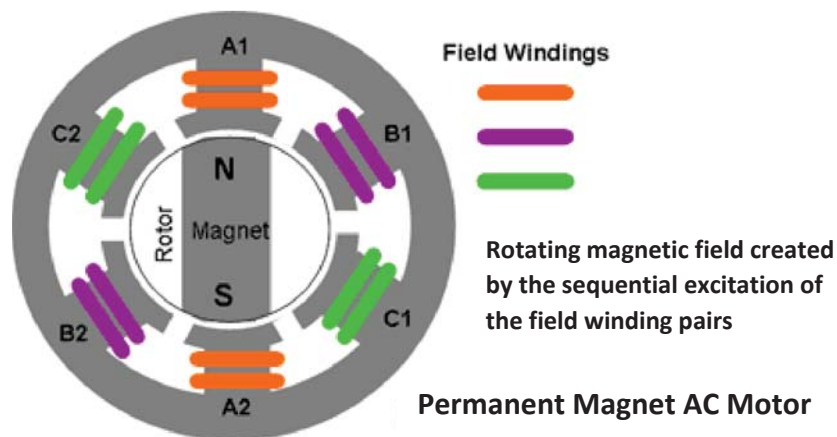


Figure 4-5: PMAC / PMSM / Brushless DC design [16]

These motors are synchronous machines, which means the mechanical speed of the rotor matches the speed of the rotating magnetic field. As field winding pair [A1, A2] in Figure 4-5 is switched off and pair [B1, B2] is switched on, the rotor rotates clockwise to align with the energised winding. It follows that increasing the number of rotor poles and winding slots increases total flux (Φ) and rate of change of flux for a given rotational speed. This means an increased magneto-motive force (MMF) and increased torque (τ):

$$MMF = \Phi R \quad \rightarrow \quad MMF \propto \Phi \quad (4-1)$$

$$\tau = k\Phi I_A \quad \rightarrow \quad \tau \propto \Phi \quad (4-2)$$

$$RPM = \frac{120f}{P} \quad (4-3)$$

However, there is a limit to increasing the pole count (P) in attempt to increase torque. Achieving the same RPM with more poles requires a higher switching frequency (f), which worsens the effects of as iron losses.

Though PMAC motors are expensive to build due to the cost of powerful rare-earth permanent magnets and require expensive controllers, they have many advantages for electric vehicles. They are low maintenance, have a high power-to-weight and power-to-size ratio, high efficiency and have controllable, constant torque across all speeds including at stall.

4.3.2 Motors for 2013 Formula SAE Car

The four motors chosen for the 2013 car were low-cost, outer-rotor, brushless PMAC machines (Turnigy CA120-70). Hooper details the considerations made to reach this decision [10]. Below is a summary of their specifications. The motors are completely independent and mounted in-hub to achieve an all-wheel-drive (AWD) vehicle.

Maximum Voltage	70 Volts
Peak Current	300 Amps
Maximum Speed	10,500 RPM
Maximum Torque	20 Nm
Motor Constant – speed	147 RPM / Volt
Motor Constant – torque	0.065 Nm / Amp
Stator Windings	24
Magnet Pole Pairs	14
Weight	2.73 kg

Table 4-1: Turnigy CA120-70 PMAC Specifications

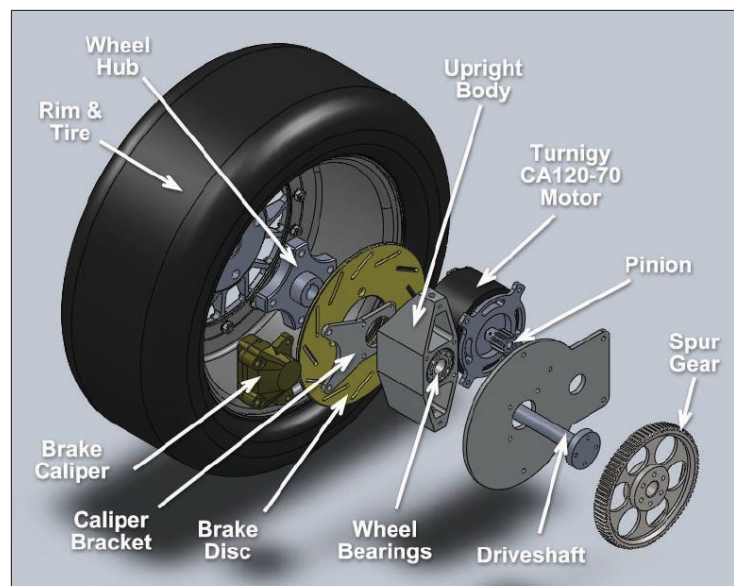


Figure 4-6: Exploded View of Wheel-Hub Assembly [10]

4.4 MOTOR CONTROLLERS

The brushless PMAC motors used in both the 2010 and 2013 Formula SAE cars require three-phase AC motor controllers to provide commutation. An electronic control system excites the windings, in turn, at specific frequencies and currents, thus controlling speed and torque. The motor controllers used to achieve this are the Kelly KBL72301X controllers; the same are used for both cars. These controllers are powered by a 48 to 60 Volt DC supply from the vehicle's the lithium ion phosphate batteries (depending on level of charge). The DC supply is connected in parallel to each of the

controllers' [B+] and [B-] posts, shown in the mechanical diagram of the controller's front panel in Figure 4-7. Three AC phases are generated, 120° apart, and are connected to the motor's three phase windings using posts [A], [B] and [C] shown in Figure 4-7.

These motor controllers are rated up to 72 Volts which is at least 10 Volts higher than the maximum battery voltage – to be safe from over-voltage damage. They are also capable of delivering 300 Amps continuous which is the absolute peak rating of the motors – guaranteeing controller overheating will not be significant. They feature regenerative braking which will help increase range and score well in the endurance event, in addition to the potential for effective ABS and EBD by electronically regulating brake force. This particular model also has peripherals to communicate over CAN bus which provides very fast and convenient access to data about the motor and controller state. Below are the low voltage signal breakouts of the Kelly motor controller and the interfacing of these signals in relation to the DCU.

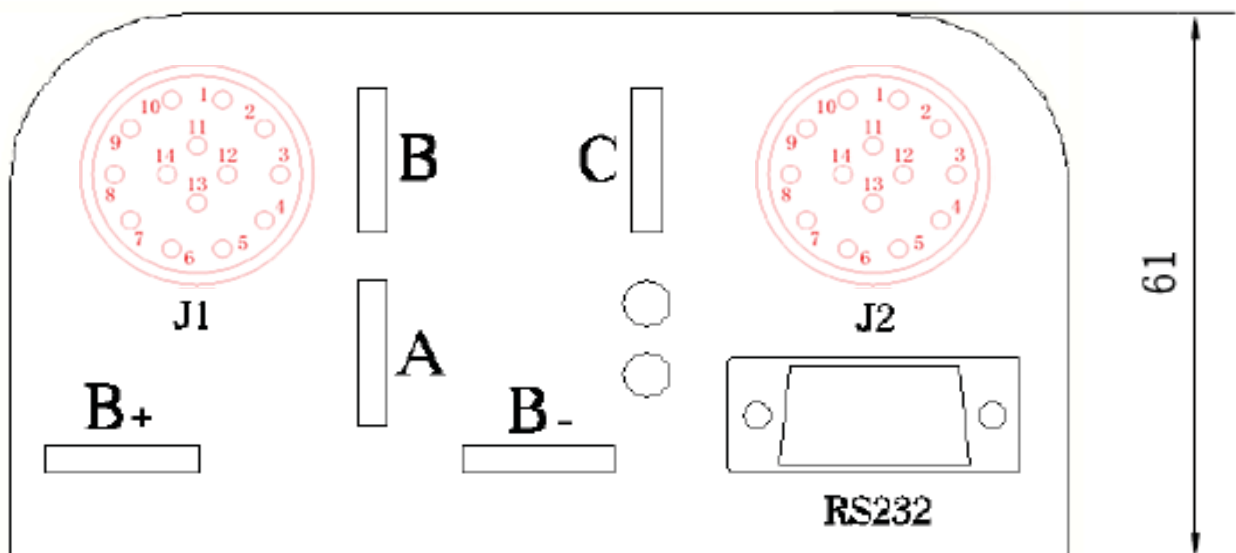


Figure 4-7: Kelly KBL72301X Motor Controller Connections Panel [17]

J1 Pin-out		Connection
1	Power supply output	Not Connected
2	Current Meter	Not Connected
3	Main Contactor	Not Connected
4	Reverse Alarm	Not Connected
5	GND	Low Voltage Ground (isolated from HV tractive system ground)
6	Green LED: On indicator	Not Connected
7	GND	Low Voltage Ground
8	RS232 Rx	Not Connected
9	RS232 Tx	Not Connected
10	CAN high	Vehicle CAN bus network – high signal line
11	CAN low	Vehicle CAN bus network – low signal line
12	Reserved	Not Connected
13	GND	Low Voltage Ground
14	Red LED: Fault indicator	Not Connected

J2 Pin-out		Connection
1	Power supply input	Low Voltage Supply (12V from DC-DC converter)
2	GND	Low Voltage Ground
3	GND	Low Voltage Ground
4	Motor temperature input	Not Connected
5	Throttle analogue input	DCU PWM output (one of the eight individual PWM channels)
6	Brake analogue input	DCU PWM output (another of the eight individual PWM channels)
7	5V supply output	Motor's Hall encoder module - 5V supply
8	Throttle active switch input	Low Voltage Ground
9	Reverse switch input	GND or floating – depending whether motor is a left or right wheel
10	Brake switch input	Not Connected
11	Hall encoder phase C	Motor's Hall encoder module – Hall-effect sensor C
12	Hall encoder phase B	Motor's Hall encoder module – Hall-effect sensor B
13	Hall encoder phase A	Motor's Hall encoder module – Hall-effect sensor A
14	GND	Low Voltage Ground

Table 4-2: Kelly KBL72301X Motor Controller Low Voltage Signals Pin-out and Connections within Vehicle

4.4.1 CAN Message Objects

The Kelly motor controllers can transmit an arsenal of information about their configuration or immediate measurements related to the controller, batteries or motor. Unfortunately, the controllers can only respond to requests for data – they cannot receive configuration parameters, commands or driver inputs. The most useful data values available for the DCU to request are summarised as follows:

CAN message (sent from DCU)	Controller's response
0x1B	Byte[0]: Analogue brake pedal input [0 – 255] Byte[1]: Analogue throttle pedal input [0 – 255] Byte[2]: Voltage of LV supply (J2 pin 1). See Figure 4-7 Byte[3]: Voltage of 5V supply for Hall sensor encoder (J2 pin 7). See Figure 4-7 Byte[4]: Voltage of HV battery – between posts [B+] and [B-]. See Figure 4-7
0x1A	Byte[0]: Phase A current Byte[1]: Phase B current Byte[2]: Phase C current Byte[3]: Phase A voltage Byte[4]: Phase B voltage Byte[5]: Phase C voltage
0x33	Byte[0]: PWM duty cycle percentage Byte[1]: 0 or 1 indicating whether or not driving is enabled Byte[2]: Motor temperature Byte[3]: Controller temperature Byte[4]: Temperature of high side FETMOS heat sink Byte[5]: Temperature of low side FETMOS heat sink
0x37	Byte[0-1]: Motor mechanical speed in RPM Byte[2]: Percentage of controller's peak rated current being utilised

Table 4-3: Summary of Most Useful Data Available on the CAN Bus

Most importantly, an accurate measurement of the mechanical speed of rotation is available over CAN bus and can be transmitted to the DCU at high-speed, taking sensor processing tasks away from the DCU. The method used by the motor controller to make this measurement of rotational speed is explained in section 4.5.1 and makes use of a three-channel Hall-effect encoder mounted on the motor.

4.4.2 Parameter Configuration

The motor controllers require configuration to operate correctly on the Formula SAE cars. Sensors also need to be calibrated and current restricted to avoid damage to motors or batteries. Kelly provides software to configure the controllers using a PC and RS232 serial.

Throttle pedal sensor

The controller can be configured to expect a 0-5V three-wire pot or around 1-4V Hall-effect sensor input for throttle position. Additionally, the effective starting and ending voltages can be set so they compensate for the dead-zones of the particular pedal used. Throttle response can be set to limit how quickly the controller responds to a change in throttle input.

Motor and battery current limits

The output current to the motor can be limited to the motor's peak rating (in this case, set to 83% to limit motor peak to 250 Amps, since no temperature monitoring is installed yet). Battery current does not need to be limited as the battery discharge rate is high enough for this load.

Battery voltage limits

To prevent damage to the batteries, upper and lower battery voltage limits can be set. The controller will disable drive if the voltage is too low and will disable regenerative braking if the voltage is too high. These have been set to 45 Volts and 65 Volts, though they are unnecessary precautions since the battery management system provides more specific protection.

Control mode

Either torque or speed control mode can be selected. For this project, the algorithm controls torque so this is the configuration used.

Regenerative braking

The controller can enable or disable the regenerative braking function and limit the maximum braking force. If enabled, it can be configured to apply braking when the throttle is released or just when the brake is pressed.

Speed limit

A speed limit can be set as a percentage of the motor's maximum possible speed. This has been left at 100%.

Number of poles

To get a correct measurement of rotational speed, number of permanent magnet poles must be set. This is configured to 28 as the motor has 14 pole pairs.

4.5 SENSORS

4.5.1 Motor Position Encoder

Brushless PMAC motors are usually controlled by two different methods – trapezoidal or sinusoidal excitation. The trapezoidal method switches the phase current direction every 120° (magnetic) and maintains 120° separation between phases. The sinusoidal method produces three identical sine waves, 120° out-of-phase.

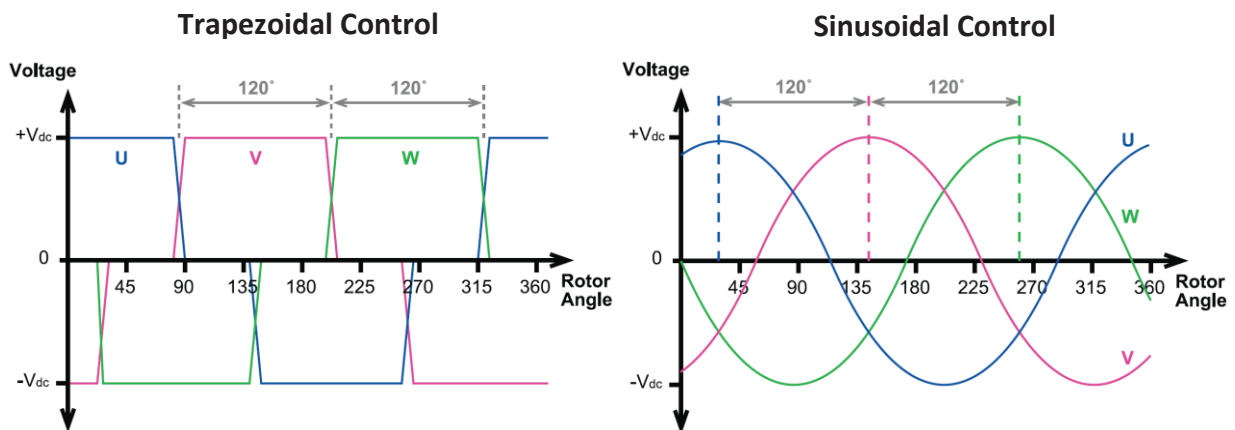


Figure 4-9: Plots of Phase Voltages for Trapezoidal and Sinusoidal PMAC Motor Control Methods [10]

In each case, the controller requires some form of feedback to know when to energise the phases. This can be done using latch-type Hall-effect sensors that alternate between digital high and low outputs as they are moved between the proximities of north and south magnetic poles. Three sensors would be required – one for each phase. In the case of the Turnigy motors (see 4.3.2), with rotor on the outside, proximity to the magnetics is easy to achieve.

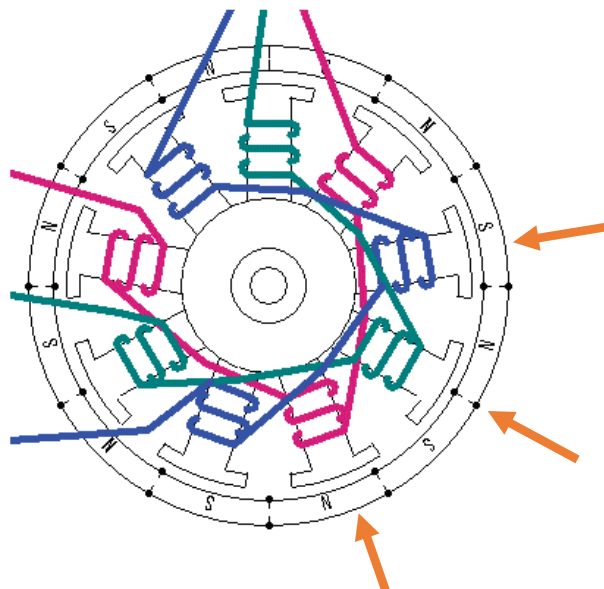


Figure 4-8: Hall-effect Sensor Placement to Determine Motor Position

The arrows in the above figure indicate possible placement of the Hall-effect sensors. The sensors must be placed multiples of 120° apart. In Figure 4-8, the sensors are placed 240° to show they can be placed relative to the stator teeth.

Turnigy CA120-70 motors have 28 magnets (14 pole pair), so the mechanical angle between each pole pair is:

$$\theta_{pp} = \frac{360}{14} = 25.71^\circ \quad (4-4)$$

The rotation from one magnetic north to the next north around the circumference is a complete cycle and therefore 360°. So this must be divided into three to get the mechanical angle of 120° magnetic.

$$\frac{\theta_{pp}}{3} = \frac{25.71^\circ}{3} = 8.5714^\circ \quad (4-5)$$

Therefore, three Hall-effect sensors must be placed at integer multiples of 8.57° apart from each other, around the edge of the motors. Since the motors have a diameter of 120mm, the arc length representing the separation between sensors is:

$$l = \theta r$$

$$l = 8.5714 \left(\frac{\pi}{180} \right) \times 0.06 = 8.9mm \quad (4-6)$$

Since most sensors are in a 4mm wide 3-pin SIP package this leaves very little room between sensors for positioning, wiring etc. Choosing 240° magnetic phase difference will result in a mechanical separation of 17.14° which is likely to be easier to fabricate. Using these calculations, a module can be built to position the Hall-effect sensors correctly around the motor. Perspex was used to fabricate the module and epoxy to fasten the sensors and wires in place.

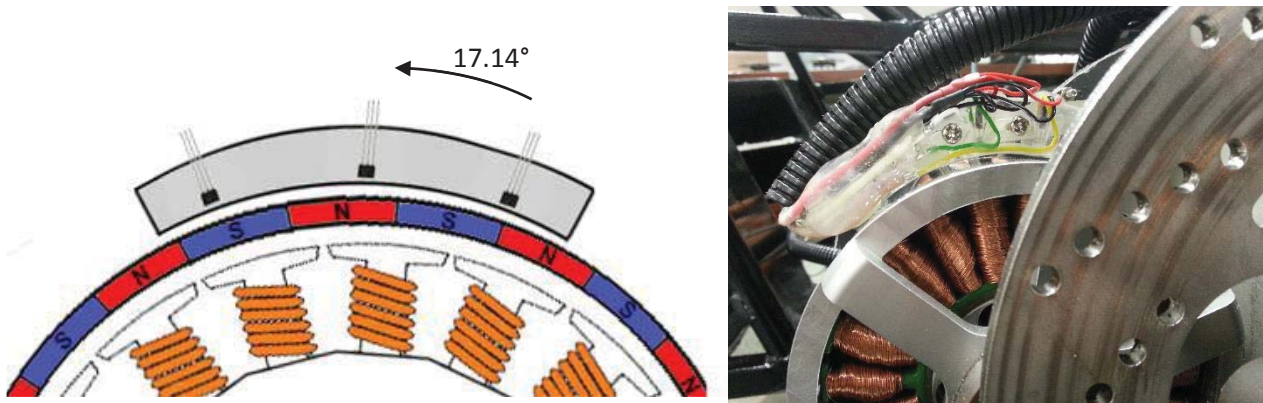


Figure 4-10: Hall-effect Motor Position Encoder

The sensors chosen were Hall-effect bipolar latch switches. The requirements on these sensors are fast switching time, automotive temperature range and sufficient sensitivity to switch with available magnetic field strength. Most of these style sensors available on the market fit the requirements and Allegro's A1220 was chosen. Electronically, the sensors require two additional components – a decoupling capacitor and a pull up resistor. SMD packages of these components were chosen and soldered directly onto the wires of the 3-wire SIP to avoid the need for additional circuits.

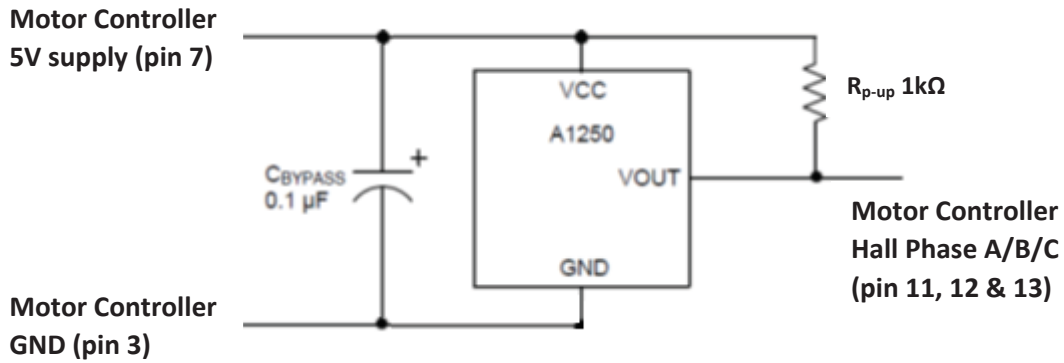


Figure 4-11: Schematic of Hall-effect Sensor Interface

With all three sensors connected and mounted, the motor was manually spun to check the signals. A two-channel oscilloscope was connected to two of the sensors in turn.

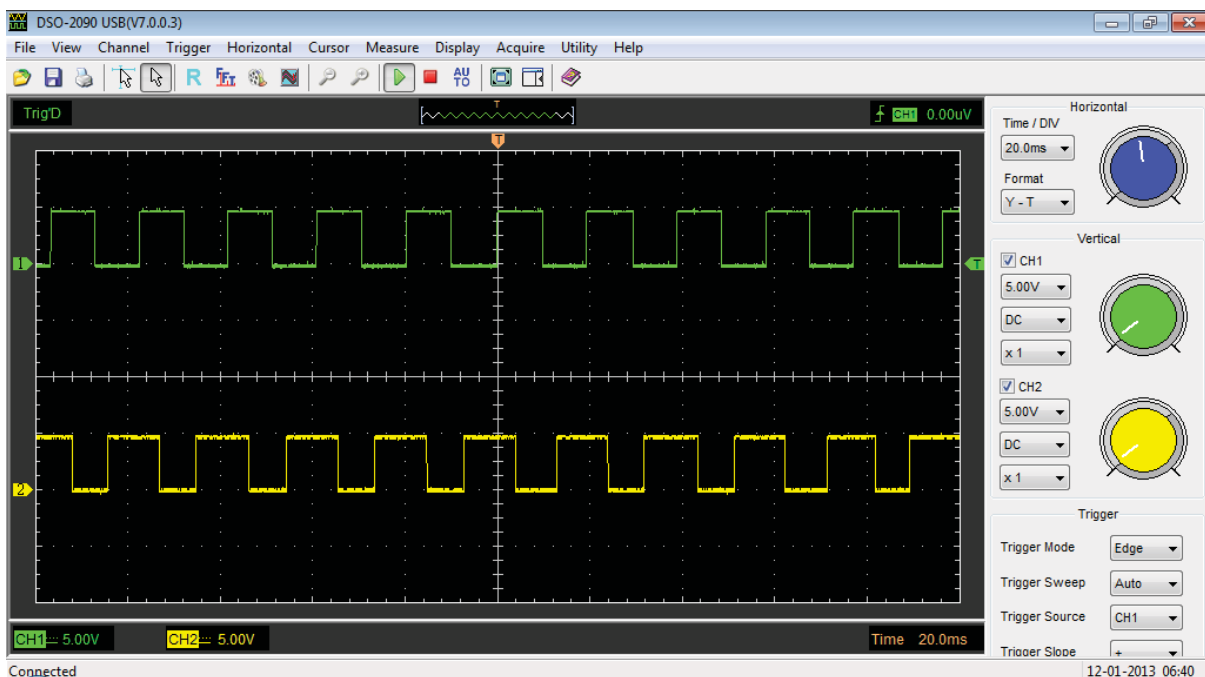


Figure 4-12: Oscilloscope Measurements of Hall-effect Encoder Channels

As can be seen in Figure 4-12, the lower waveform (channel 2) is phase-shifted left by precisely a third of a cycle. Both waveforms have clean edges and are approximately 50% duty cycle, as required. Since only a two-channel oscilloscope was available, each of the three combinations of two sensors were tested in turn for a phase difference of 120°.

In addition to providing the motor controllers with rotor position feedback in order to energise windings at the correct time, the sensor modules allow the controller to very precisely measure the speed of rotation. This speed measurement is available as a CAN message object (see section 4.4.1) which is more accurate and less processor demanding for the DCU than most other cost-effective options for wheel speed sensing.

4.5.2 Steering encoder

A measurement of steering angle is required for the DCU algorithm. Requirements are a low-cost, durable sensor, not susceptible to vibrations and physical shocks. A number of different options and mounting positions were considered.

Linear potentiometer



Figure 4-13: Linear Potentiometer [18]

A linear potentiometer mounted to the steering rack would have the advantage of high precision and repeatability. It would also be measuring closer to the wheel and therefore not affected by any play in the spline connecting the steering column to the rack. Interfacing the sensor with the DCU would simply require connection to an ADC channel. The Cortex-M3 is capable of a maximum 10-bit resolution at 500,000 samples per second which is excessively fast but limited to 1024 steps, assuming steering lock-to-lock utilises the full travel of the potentiometer.

This sensor is an extremely expensive option and they are delicate, easily damaged instruments. This is especially problematic since it would be mounted on the steering rack near the driver's feet – requiring proper casing to protect.

Rotary potentiometer



Figure 4-14: Rotary Potentiometer [19]

Using gears or a pulley to couple, a rotary potentiometer could be mounted adjacent to the steering column. This solution is not very expensive but requires precise design and mounting so that gears or pulley do not slip in response to vibration or shock. Also, precautions must be taken in designing the coupling system to ensure extra play isn't added in addition to the steering column's spline play, distorting measurements. As with the linear potentiometer, the 3-wire sensor is interfaced with the DCU's ADC input and is limited to a resolution of 1024 steps. This sensor is not as delicate as a linear potentiometer and is less susceptible to physical damage.

Contactless optical quadrature encoder

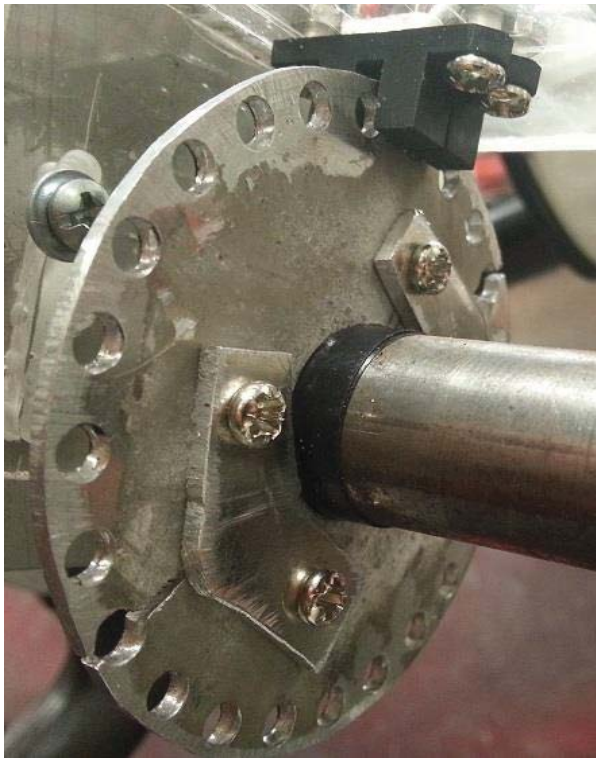


Figure 4-15: Optical Quadrature Steering Angle Encoder



Figure 4-17: Photo Interrupter [20]

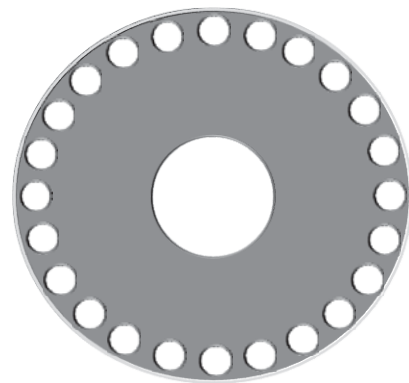


Figure 4-16: Encoder Wheel

Ultimately, the contactless incremental encoder was chosen due to its extremely low cost, room for movement in response to vibration and shock, low wear and maintenance, and flexibility in designing resolution. The DCU has an on-board quadrature interface, so additional signal processing is not required.

An optical incremental encoder works by using a photo interrupter (Figure 4-17) and a code wheel (Figure 4-16). As the wheel rotates, it interrupts the light – producing an output of rising and falling edges. With a single photo interrupter, angle and speed of rotation can be measured but only in the same direction; a change of direction cannot be detected. A quadrature encoder, however, uses two photo interrupters, positioned 90° out-of-phase producing the following waveforms:

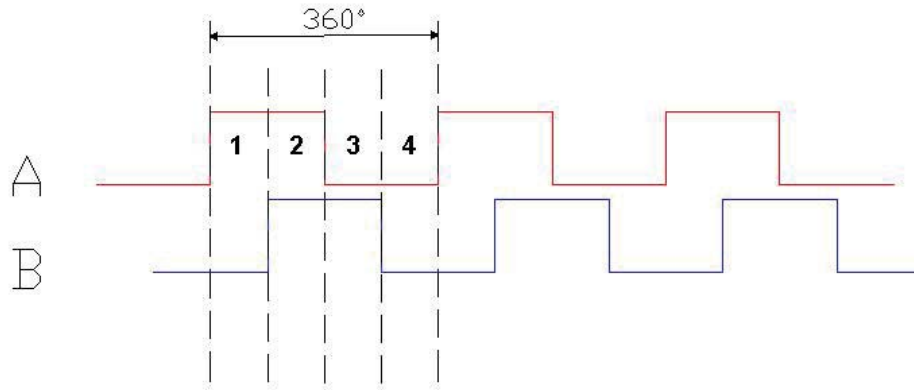


Figure 4-19: Quadrature Encoder Photo Interrupter Signals

STATE	CHANNEL A	CHANNEL B
1	High	Low
2	High	High
3	Low	High
4	Low	Low

Table 4-4: Quadrature State Table

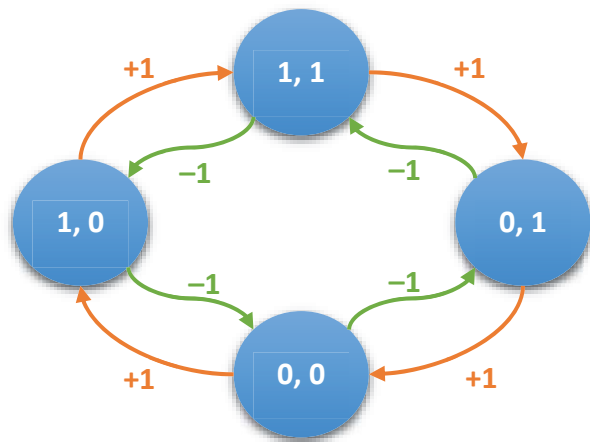


Figure 4-18: Quadrature Moore Machine

Positioning the photo interrupters in this way results in four unique states per cycle, as shown in Table 4-4. Each state can only transition to two other states – one transition corresponding to a clockwise movement (increment) and the other corresponding to an anticlockwise movement (decrement). In addition to the ability to count edges incrementally in both directions, the quadrature system has four edges per cycle instead of two, doubling the resolution of the encoder.

The mechanical drawings of the photo interrupters were consulted (see Appendix 8.1) in order to space the sensors correctly and fabricate the code wheel. When placed flush side-by-side, there is precisely 6mm between the optical lines of the sensors. For the sensors to produce waveforms 90° out-of-phase, this 6mm must correspond to ¼ of a cycle or ¾ of a cycle (or 1 ¼, 1 ¾, etc.). Therefore, each cycle (distance between hole centres) must have a length of $\frac{6}{0.25} = 24mm$, or $\frac{6}{0.75} = 8mm$, or $\frac{6}{1.25} = 4.8mm$, $\frac{6}{1.75} = 3.4mm$, etc. A cycle length of 8mm was chosen as this size is realistic to fabricate with accuracy. Also, due to space limitations, the disk cannot be greater than 65mm. The code wheel design was therefore a 61mm diameter disk using 2mm thick aluminium with 24 equally spaced 4mm holes just inside the edge, as shown in Figure 4-15 and Figure 4-16. With the quadrature system producing four counts per cycle, the resulting resolution using the 24-hole code wheel is 96 counts per revolution, or $\frac{360}{96} = 3.75^\circ$.

The sensors can be interfaced directly with the DCU as the photo interrupter modules contain Schmitt triggers to produce clean edges without needing additional circuitry (see schematic Figure

4-20). The on-board quadrature peripherals and associated libraries process the digital interrupts on rising and falling edges, and consult the Moore machine shown in Figure 4-18 to increment or decrement a counter stored in a register for access elsewhere in the code.

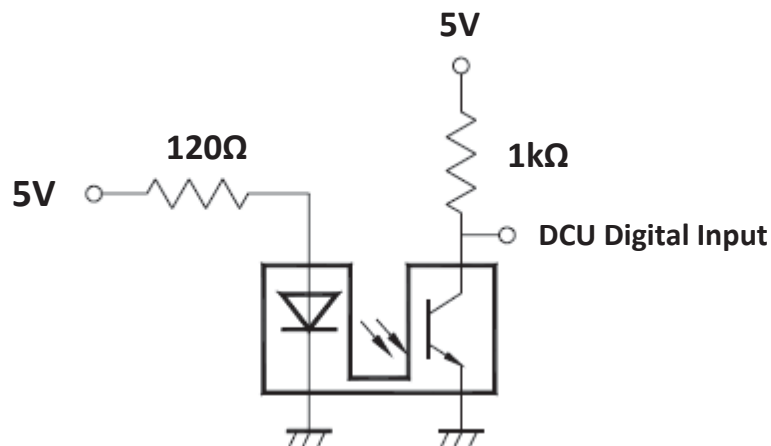


Figure 4-20: Schematic of Photo Interrupter with Connections to DCU

4.5.3 IMU



The Inertial Measurement Unit provides the DCU with acceleration measurements and yaw rate. A low-cost module based on the InvenSense ITG3200 and Analog Devices ADXL345 was chosen, though this will be replaced by a more accurate device when budget allows. The module is powered off a 3.3V supply and outputs analogue voltage levels reflecting three axes of linear acceleration and three axes of angular velocity. The voltages can be read by the DCU using the ADC inputs. The IMU is positioned in the centre of the vehicle under the driver’s seat so inertial measurements are made from as near as possible to the centre of mass of the vehicle.

4.5.4 Accelerator and Brake Pedals



Figure 4-21: Hall-effect Accelerator Pedal [21]

The Formula SAE electrical rules require a foot-activated throttle demand with at least two separate sensors having independent power supplies. A commercial pedal was chosen that utilises two Hall-effect sensors. The advantages of this decision include sensor reliability and time saved in design process. The output signals are 0.8 Volts to 4.5 Volts and can be wired directly to the DCU’s ADC inputs.

The brake pedal has been fabricated to suit the master cylinder chosen for the brake system. Two Hall-effect sensors mounted on the chassis and permanent magnets mounted on the pedal facilitate brake position measurement.

5 TEST RESULTS

The 2013 Formula SAE car had its first drive on March 10th, 2013. At this point the vehicle was well behind schedule and over-budget. It drove a lap and a half of the track before mechanical faults were observed and driving ceased. It has not yet returned to a driving state due to a number of redesigns required including new, stronger drive shafts and different suspension. As such, the planned tests for the AWD algorithm could not be performed. In an attempt to prove the concept with whatever resources were available, the algorithm was modified for and hardware implemented on a RWD version of the Formula SAE platform that the REV team completed in previous years. This was not ideal but provided an opportunity to prove the effectiveness of the system.

The 2010 RWD Formula SAE car has a significantly heavy rear and has a tendency of understeering due to the reduced down-force at the front. Correcting for this understeer and thus improving cornering performance was therefore the primary goal of this test.

5.1 THE TEST PROCEDURE

In order to test the vehicle's cornering performance under controlled conditions, a circle of cones was laid out with a 6m radius. The vehicle was driven around this circle, therefore holding a constant steering angle, while the throttle was ramped up gradually. The speed was increased until the point that the vehicle lost stability by either spinning out or understeering too much to be realistically following any sort of cornering path.

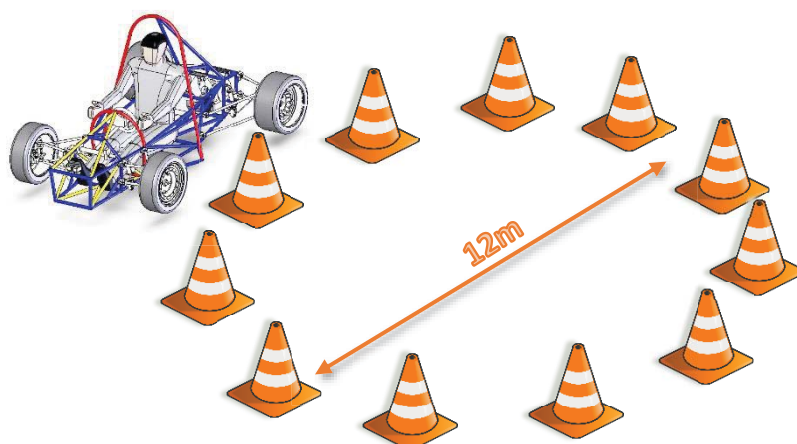


Figure 5-1: Test Track for Cornering Performance

The test was performed a number of times with the torque vectoring algorithm disabled and a number of times with it active. All sensor was logged during each test. It was predicted that understeer would be slightly corrected for by the algorithm and faster speeds could be achieved, however it was assumed that the driver wouldn't observe much of a change; any improvements were more likely to be observed during data analysis.

5.2 RESULTS

The data was processed in Excel and selections made from the extreme quantities of data. Two of these selections are shown below – one without torque vectoring and the other with.

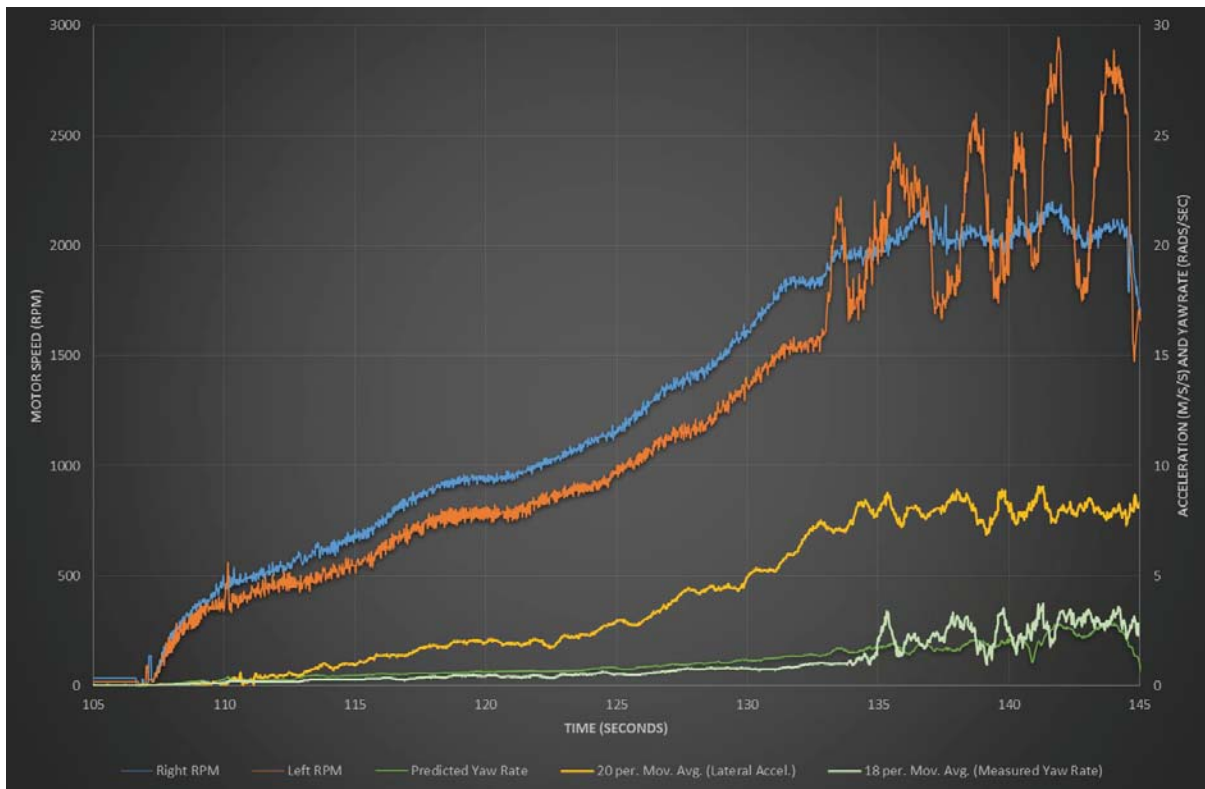


Figure 5-2: Plot of Test Results with Torque Vectoring DISABLED

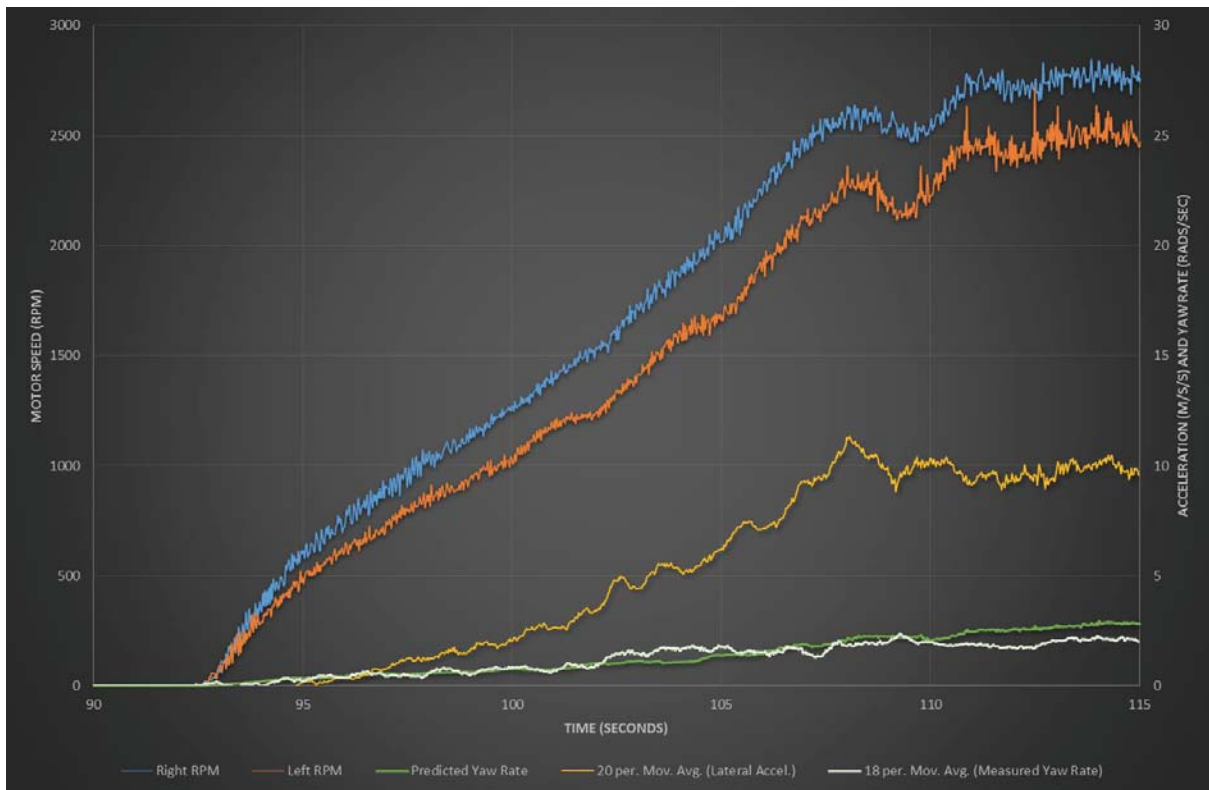


Figure 5-3: Plot of Test Results with Torque Vectoring ACTIVATED

The most striking observation of the above plots was the definitive point at which the trends change. In Figure 5-2 this is at approximately $t = 130$ seconds and in Figure 5-3, approximately $t = 109$ seconds. In the test without the torque vectoring system active, it is most evident that stability has been lost. The inner wheel (orange) is oscillating as it gains and loses traction repeatedly – it is attempting to drive with more torque but does not have enough friction force. Less torque should be applied to this wheel and instead more to the outer wheel. A varying amount of understeer was noticed in all tests and this can be seen in the plots, where the predicted yaw rate (desire yaw rate) often exceeds the actual measured rate.

Also interesting to note is the lateral acceleration measurement. In Figure 5-2 with no torque vectoring, a maximum lateral acceleration of around 8m/s/s was achieved before stability was lost. In Figure 5-3, around 10m/s/s was reached with the torque vectoring system active.

The most satisfying observation overall from the above plots is the clear increase in achieved motor speed from around 2000 RPM to around 2500 RPM. In terms of vehicle velocity, the data suggests an increase from around 10.5 m/s to 12.3 m/s (38 km/h to 44 km/h) or approximately 17%.

5.3 CONCLUSIONS

As predicted, improvements were hard to observe during the test itself but from the data it can be seen that the torque vectoring system is effective. Understeer is still evident but the system was able to vector torque away from the inside wheel while cornering and increase outside wheel torque where it could be utilised. More test situations would show additional effectiveness, such as a chicane test or double-lane-change test. Even with the 2WD simplification of the algorithm, it is clear that a 17% increase in cornering speed for a given 6m radius is a valuable improvement in performance. The results of this test could be extrapolated to suggest improvement in handling would be observable when the system is tested on the 2013 AWD car.

6 FUTURE IMPLEMENTATION, FURTHER RESEARCH AND CONCLUSIONS

The promise of this project could inspire many different avenues of research and refinement in the area. Obviously the first step is to test the system on the 2013 AWD car and see if similar improvements are achievable. A more accurate IMU would be the next logical step, as the device used in the current system is very limiting. Ideas were considered for a driver heads-up-display with the most immediately relevant information provided in addition to display of any DCU-specific diagnostics and enabling live parameter modification. A trackside PC that communicates wirelessly with the vehicle could help make refinements and bring problems to the team's attention. There are also a lot of CAN message objects that weren't made use of in this project but may be relevant to a trackside observer. Ultimately, there is a huge potential for all kinds of experimentation as most drive-control algorithms simply require a software update with the new ideas rather than mechanical redesign.

It is reasonable to suggest that though this project has had its set-backs, the torque vectoring system designed is supported by existing research and through preliminary testing, its concept proves effective for a RWD electric vehicle. Results thus far demonstrate improved stability during cornering and would likely be improved further on the full AWD implementation.

Electric vehicles should not be overlooked as they have the advantage in this area of competitive design due to characteristics like superior torque curves, precise controllability and responsiveness, better flexibility of design and control of weight distribution. If it wasn't for today's battery technology limitations, it would be reasonable to assume that specifically-designed electric performance vehicles could out-perform similar combustion engine alternatives, whilst representing a cleaner, more sustainable mode of transport.

7 REFERENCES

- [1] C. Burt, X. Piao, F. Gaudi, B. Busch, and N. F. N. Taufik, "Electric Motor Efficiency under Variable Frequencies and Loads," in *Journal of Irrigation and Drainage Engineering*, vol. 134, no. 2, 2008, pp.129-136
- [2] Image Credit. EE Times. <http://www.eetimes.com/design/automotive-design/4207237/Is-there-a-future-for-hybrid-vehicles--Part-1?pageNumber=1>.
- [3] Y. Hori, Y. Toyoda, and Y. Tsuruoka, "Traction control of electric vehicle: basic experimental results using the test EV "UOT electric march",," in *Industry Applications, IEEE Transactions*, 1998, vol. 34, no. 5, pp.1131–1138.
- [4] SAE International, "2013 Formula SAE Rules," <http://students.sae.org/competitions/formulaseries/rules/>
- [5] M. K. Park, I. H. Suh, S. J. Byoun, and S. R. Oh, "An intelligent coordinated control system for steering and traction of electric vehicles," in *Proc. IEEE IECON 22nd Int Industrial Electronics, Control, and Instrumentation Conf*, 1996, vol. 3, pp. 1972–1977.
- [6] Yongli Zhao, Yuhong Zhang, and Yane Zhao, "Stability control system for four-inwheel-motor drive electric vehicle," in *Proc. Sixth Int. Conf. Fuzzy Systems and Knowledge Discovery FSKD '09*, 2009, vol. 4, pp. 171–175.
- [7] D. Piyabongkarn, R. Rajamani, J.Y. Lew, and Hai Yu, "On the use of torque-biasing devices for vehicle stability control," in *American Control Conference*, 2006, june 2006, pp.5360-5365
- [8] J. Wang, Q. Wang, L. Jin, C. Song, "Independent wheel torque control of 4WD electric vehicle for differential drive assisted steering," in *Mechatronics*, vol.21, no. 1, February 2011, pp.63–76
- [9] N. Ando and H. Fujimoto, "Yaw-rate control for electric vehicle with active front/rear steering and driving/braking force distribution of rear wheels," in *Advanced Motion Control, 2010 11th IEEE International Workshop on*, march 2010, pp. 726–731.

- [10] I. Hooper, "Development of In-Wheel Motor Systems for Formula SAE Electric Vehicle," Thesis. University of Western Australia, Perth, 2011.
- [11] Z. Brandstater, "Traction Control and Torque Vectoring with Wheel Hub Motors," Thesis. University of Western Australia, Perth, 2011.
- [12] R. Pusca, Y. Ait-Amirat, A. Berthon, and J. M. Kaučmann, "Modeling and simulation of a traction control algorithm for an electric vehicle with four separate wheel drives," in *Proc. VTC 2002-Fall Vehicular Technology Conf. 2002 IEEE 56th*, 2002, vol. 3, pp. 1671–1675.
- [13] Image Credit. <http://ars.els-cdn.com/content/image/1-s2.0-S1569190X11001237-gr3.jpg>.
- [14] Image Credit. <http://therevproject.com/>
- [15] Image Credit. <http://www.mpoweruk.com/motorsbrushless.htm>.
- [16] Kelly Controllers. "Kelly KBL Brushless Motor Controller User's Manual," <http://kellycontroller.com/support.php>
- [17] Image Credit. http://www.bmotorsports.com/shop/product_info.php/products_id/1329.
- [18] Image Credit. https://www.egr.msu.edu/eceshop/Parts_Inventory/totalinventory.php.
- [19] Image Credit. <http://www.altronics.com.au/index.asp?area=item&id=Z1670>.
- [20] Image Credit. http://www.evsource.com/tls_throttle_pedal.php.

8 APPENDICES

8.1 EXTRACT FROM BPI-3C1-13 PHOTO INTERRUPTER DATASHEET



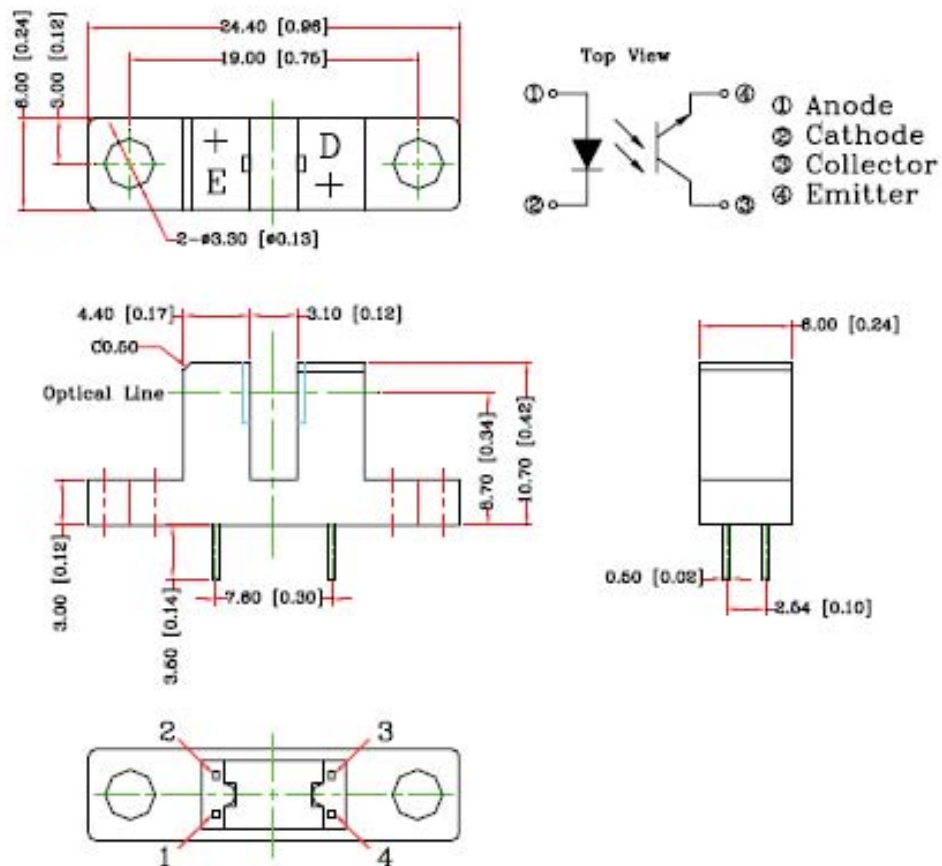
BRIGHT LED ELECTRONICS CORP.

BPI-3C1-13

● Features:

- * Non-contact switching.
- * For direct pc board or dual-in-line socket mounting.
- * Fast switching speed.
- * This product doesn't contain restriction substance, comply ROHS standard

● Package Dimensions



Notes:

1. All dimensions are in millimeters(inches).
2. Tolerance is $\pm 0.25\text{mm}$ unless otherwise specified.
3. Lead spacing is measured where the leads emerge from the package.
4. Specifications are subject to change without notice.

REV:1.3 Page 1 of 5